FACULTY
OF APPLIED SCIENCES
UNIVERSITY
OF WEST BOHEMIA

DIPLOMA THESIS

Double pendulum contact problem

Bc. Jan Špička

Plzeň, May 31, 2013

Contents

1 Introduction **9**

2 Literature review **11**

2.1 Motivation for impact biomechanics 11

2.2 Contact detection and minimum distance 11

2.2.1 Surface approximation 11

2.2.2 Contact detection 12

2.2.3 Minimum distance calculation 13

2.3 Contact force models 16

2.3.1 Discrete contact model 17

2.3.2 Continuous contact model 20

3 Method **25**

3.1 Double pendulum model 25

3.1.1 Local and global coordinate systems 25

3.1.2 Spatial motion implementation 26

3.1.3 Equation of motion 29

3.1.4 Kinematics constrains definition 31

3.1.5 Numerical solution 35

3.2 Contact calculation 37

3.2.1 Minimum distance problem application 38

3.2.2 Contact force 43

3.3 Contact parameters optimization 48

3.3.1 Bouncing ball theory 51

3.3.2 *IF* problem 53

3.3.3 Numerical optimization 55

4 Results and discussion **57**

4.1 Free double pendulum motion 57

4.2 Arm gravity motion 59

4.3 Numerical optimization 62

4.3.1 Hertz's model 62

4.3.2 Spring-dashpot model 63

4.3.3 Non-linear model 64

4.3.4 Summary of optimization 65

4.4 Contact force 66

4.5 Double pendulum contacting a plain 67

4.6 Legform impactor 69

5 Conclusion **72**

References **74**

List of Figures

2.1 Line approximation of bodies [18] 12
2.2 Two (a) disjoint and (b) overlapping ellipsoids and corresponding $f(\lambda)$ [21] 13
2.3 Impact of two bodies [3] 16
2.4 Loading and unloading phases of discrete contact model 17
2.5 Equivalent system [9] 21
2.6 Contact force history for the spring-dashpot model [3] 22

3.1 Local and global coordinate systems 26
3.2 Double pendulum 27
3.3 Spherical joint 27
3.4 Two balls collision 37
3.5 Parallel plains 38
3.6 Acting normal contact force 44
3.7 Two equivalent systems 45
3.8 Flowchart of ODE solution 47
3.9 Flowchart of optimization 49
3.10 Bouncing ball example [9] 50
3.11 Ball position [9] 50
3.12 Contact force discontinues 54

4.1 Position of double pendulum at t=0 sec 58
4.2 Position of double pendulum at t=0.5 sec 58
4.3 Position of double pendulum at t=1sec 58
4.4 Position of double pendulum at t=1.5 sec 58
4.5 Position of double pendulum at t=2 sec 58

4.6 Position of double pendulum at t=2.5 sec 58
4.7 Passive bending moment of a shoulder 59
4.8 Passive bending moment of an elbow 59
4.9 Passive bending moment of a wrist 59
4.10 Initial position of arm 60
4.11 Comparison of trajectories of an elbow 61
4.12 Comparison of trajectories of a wrist 62
4.13 Result of bouncing ball example regarding Hertz's model for $k_h = 10000$ . . 63
4.14 Result of bouncing ball example regarding Spring dashpot model 64
4.15 Result of bouncing ball example regarding non-linear damping model . . . 65
4.16 Contact force versus time 66
4.17 Position of double pendulum contacting a plain at t=0 sec 68
4.18 Position of double pendulum contacting a plain at t=0.25 sec 68
4.19 Position of double pendulum contacting a plain at t=0.5 sec 68
4.20 Position of double pendulum contacting a plain at t=0.75 sec 68
4.21 Position of double pendulum contacting a plain at t=1 sec 68
4.22 Position of double pendulum contacting a plain at t=1.25 sec 68
4.23 Experimental leg impactor [24] 69
4.24 Position of leg impactor at t=0 sec 71
4.25 Position of leg impactor at t=0.05 sec 71
4.26 Position of leg impactor at t=0.1 sec 71
4.27 Position of leg impactor at t=0.15 sec 71
4.28 Position of leg impactor at t=0.2 sec 71
4.29 Position of leg impactor at t=0.25 sec 71
4.30 Position of leg impactor at t=0.3 sec 71
4.31 Position of leg impactor at t=0.35 sec 71
4.32 Position of leg impactor at t=0.4 sec 71

List of Tables

3.1 Calculation time of identical simulation with different solvers 56

4.1 Geometric parameters of the bodies 59
4.2 Parameters of best design for SD model 63
4.3 Parameters of best design for NL model 64
4.4 Maximum values of contact force 66
4.5 Geometric parameters of the bodies 67
4.6 Geometric parameters of leg impactor 70

Annotation

The thesis concerns contact problem focused on biomechanical systems modelled by multibody approach. The example is modelling impact between human body and infrastructure. The work firstly presents algorithms for collision detection and for calculation of minimum distance, respectively. In the thesis the analytical method using tangential plain perpendicular to initial one is analysed. The Hertz, the spring-dashpot and the nonlinear damping contact force models are applied in approximation of the contact force, generated during the impact of bodies. Later on, numerical optimization method is put upon bouncing ball example. The difference between initial experiment and simulation curves is desirable to be minimise. Purpose of optimization is to find the most corresponding results of simulation to an original experiment. As consequence of these, adequate parameters of all the three contact force models are calculated. Derivation of double pendulum equation of motion is performed using Lagrange equation of second kind. Generalized force vector concerns the force, generated in case of impact performance scenario. Various of possible biomechanics applications such as motion of arm and legform impactor are developed for the purpose to motivate engineers for further studies.

Key word: Double pendulum, multibody approach, contact force models, minimum distance problem, contact force parameters, biomechanics applications

Anotace

Práce se věnuje kontaktním problémům biomechanických systémů modelovaných pomocí přístupu multi-body. Příkladem je modelování nárazu lidského těla do infrastruktury. Práce se nejprve věnuje algoritmům pro detekci kolize a pro výpočet minimalní vzdálenosti. V práci je popsána analytická metoda využívající tečné roviny rovnoběžné s původní. Hertzův model, model pružina-tlumič a model s nelineárnim tlumením jsou využity pro aproximaci kontaktní síly, generované srážkou těles. Dále je aplikován proces numerické optimalizace na příkladu skákajícího míčku. Rozdíl mezi křivkami simulace a experimentu je minimalizován za účelem nalezení řešení, které se bude nejlépe blížit danému experimentu. Výsledkem optimalizace jsou příslušné parametry všech tří modelů kontaktní síly. Pro odvození pohybové rovnice dvojkyvadla je využito Lagrangeových rovnic druhého druhu. Vektor zobecněných sil zahrnuje sílu vzniklou v případě impaktu. Možné aplikace do oblasti biomechaniky, jako je pohyb horní končetiny a impaktor lidské nohy jsou ukazány za účelem motivace k dalšímu vývoji.

Klíčová slova: Dvojkyvadlo, multibody přístup, modely kontaktní síly, minimalní vzdálenost, parametry kontaktní síly, aplikace v biomechanice

Declaration

I hereby declare that this diploma thesis is completely my own work and that I used only the cited sources.

Pilsen, May 31, 2013

Jan Špička

Chapter 1

Introduction

Impact of biomechanics studies to the consequences to the human body impact like a car crash, a pedestrian impact, falls and sports injuries. This field motivates engineers and designers to develop better safety systems for people exposed to an impact injuries. Anyone who drives a car or plays any sport is directly benefiting from impact biomechanics research.

Virtual human body models start to play an important role in the impact biomechanics. There are several approaches to develop and run such numerical models. Since the simple, usually articulated rigid body models, can evaluate mainly global human body kinematics under external loading. Detailed deformable models can even simulate tissue injuries. However the detailed models spend a lot of computational time. So the articulated rigid body models are usually sufficient tool for the first approximation and these might predict long duration global human behaviour, in very short computational time. For such models, contact modelling and contact parameters optimization are crucial aspects of a successful descriptions of a human behaviour under external impact loading. Multibody approach based on rigid bodies linked to the open kinematics chain speeds up the calculation even more. The aim of this thesis is to test the contact algorithm in the double pendulum contact problem and analyse the results.

The thesis focuses firstly on review of published researches dealing with contact mechanics problem. Algorithms for collision detection and for calculation of minimum distance between two bodies are summarized in the Chapter 2. This chapter includes also a review of contact force approaches. Differences between discrete and continuous contact models, their advantages, disadvantages and possibilities of application are discussed.

Chapter 3 describes a double pendulum as a simple articulated rigid body system based on multi-body approach. Author uses Lagrange's equation with multipliers to evaluate equation of motion of double pendulum. Derivation of impact algorithm based on multibody approach using contact force models is demonstrated. The three contact force models are Hertz's model, spring-dashpot model and nonlinear damping model, respectively. Later on, principle of numerical optimization is applied on simple contact mechanics example

of a bouncing ball. The purpose of the optimization is to evaluate contact parameters according to the behaviour of a real system.

In Chapter 4 results of particular calculations and simulations are displayed. Free motion of double pendulum is presented to be a sufficient model of human arm. Trajectories of elbow and wrist are compared with curves of 2D approach model of human arm and also with experiment. Optimized values of contact force parameters are used in bouncing ball example and the results of simulations are provided. Possibilities of further biomechanics applications are demonstrated on experimental leg impactor. Impactor can be simply modelled to be a system of two linked ellipsoid and these are getting into impact with a plain. Chapter 5 concludes the thesis.

Chapter 2

Literature review

2.1 Motivation for impact biomechanics

Impact, or contact, is a complex phenomenon that occurs, when at least two bodies undergo a collision, see Fig. 2.3. Impact (or contact) problem arise in many engineering applications, such as multi-body dynamics, robotics, aircraft, biomechanics and many others. An impact is defined as the collision of two bodies that occur over a significantly short time interval. One can characterize the impact to be a scenario presenting by large reaction forces, rapid energy dissipation and very high decrease and increase of accelerations.

2.2 Contact detection and minimum distance

Computing the minimum distance between two object of arbitrary shape is very important and it is deeply associated with impact applications. Ellipsoids are frequently used for particular shape representation for many natural organism, such as segments of human body.

There are many efficient algorithm for collision detection and related minimum distance calculation between objects. Generally there are two approaches. The first one only provides information, whether the bodies are separated, contacting at one point or the bodies are in collision, such as [2, 21]. The second one concerns algorithm, which is computing distance between bodies, respectively between surfaces [18, 21, 19].

2.2.1 Surface approximation

Sohn [18] presents an algorithm for computing distance between two free surfaces. The main idea is using line geometry to approximate shape, see Fig. 2.1, of bodies to reformulate the distance calculation problem to intersection between surfaces. By using line

geometry, one can reduce the number of variables and number of equations, that are solved. For example, two ellipsoids distance calculation problem implies four equations in four variables. This approach transforms it in a two equations in two variables system.

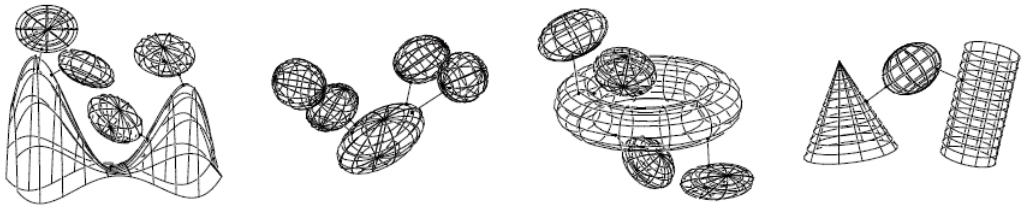

Figure 2.1: Line approximation of bodies [18]

Three main aspects of this particular method are pointed out. Let us summarise line coordinates in three dimensional space and hints how to express arbitrary surface using homogeneous coordinates associated with the Cartesian coordinate system. Let us consider arbitrary surface in the three dimensional space. Each point on this surface may be associated with a normal line through this point which is spanned by normal vector. These lines formulate two dimensional system of lines called congruence. Parametric and implicit representation of normal congruence is described and sort of basic examples are demonstrated. Minimum distance between two bodies is computed to be a minimum distance between boundaries of such surface.

To sum up this methods:

1. Generate a line coordinates of normal congruence of the surfaces. Calculate two two dimensional surfaces, which are releases with particular quadratics.
2. Calculate an intersection of two normals congruence in order to find joint normal of both surfaces. This considers finding intersection of two two dimension surfaces.
3. Find two foot points of all joint normals and check the minimum distance.

Sohn is considering the solution of the problem of minimum distance between two ellipsoids.

2.2.2 Contact detection

Wang [21] presents efficient and accurate algorithm for detection of collision in case of two moving ellipsoids. This work contains two approaches, namely a simple algebraic test for disjunction of two ellipsoids and a method for separating plain construction. Compared with tetrahedron surface approximation algorithm, this algorithm reduces calculation time and has a higher accuracy.

Collision detection

Interiors of two ellipsoids $\boldsymbol{A}$ and $\boldsymbol{B}$ are represented by matrix equations $X^T AX < 0$ and $X^T BX < 0$ respectively where A and B are real symmetric matrices of dimension equal to 4 and $X = [x, y, z, w]^T$ expresses a point in homogeneous coordinates.

A simple algebraic test for separating of two ellipsoids is established by giving two surfaces $\boldsymbol{A} : X^T AX = 0$ and $\boldsymbol{B} : X^T BX = 0$ and the quartic equation $f(\lambda) = det(\lambda A - B)$. This quantity is called characteristic equation of $\boldsymbol{A}$ and $\boldsymbol{B}$.

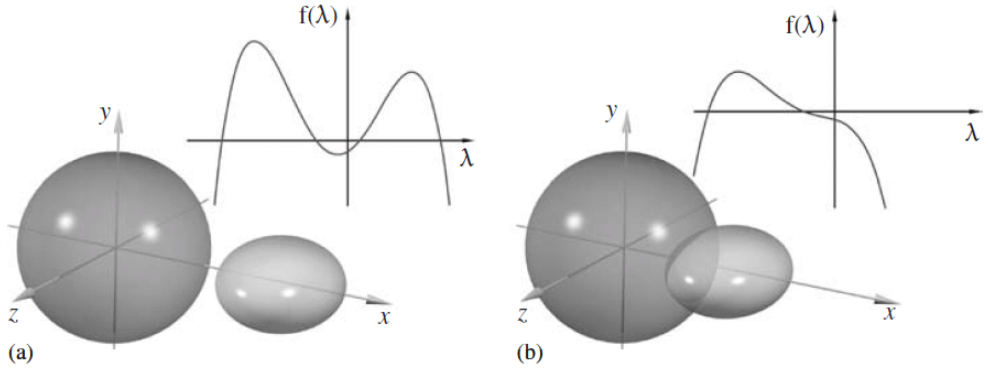

Figure 2.2: Two (a) disjoint and (b) overlapping ellipsoids and corresponding $f(\lambda)$ [21]

This two ellipsoids are disjoint if and only if equation $f(\lambda) = 0$ has two distinct positive roots. They touch each other in a single contact point if $f(\lambda) = 0$ has one positive double root. Note that ellipsoids are in contact, if the characteristic equation has no positive roots, see Fig. 2.2.

2.2.3 Minimum distance calculation

Constructing of a separating plain

Wang [21] is demonstrating how to construct a plain, which is separating two ellipsoids. Since the plain is separating the bodies, there can be no collision between ellipsoid until one of them impacts with the plain. Wang is applying affine transformation to plain and ellipsoid problem to reduce it to a problem of a sphere and a plain. Afterwards the problem of calculation between the sphere and the plain becomes a problem of distance between the centre of the sphere and the plain. However, generally speaking, affine transformation does not keep the distance magnitude, hence the truthfulness of this method can be discussable and should be proved. Due to this fact, constructing a separating plain will not be subjected to further studying . It can be observed in [21].

Pedestrian model

Moser [12] is presenting precise model of a human body for contact with vehicle application in his work. Pedestrian model is coming into contact with a rigid surfaces of the form of the car, and subsequent motion of human model is developed. Moser is using iteration process for testing distance between the surfaces of the bodies. Although precise algorithm is not reported, distance between any two points of bodies is checked and the minimum distance is determined. This algorithm can be efficient for simple geometry, which does not require high number of points.

Quadratics equation of ellipsoid

Eberly [2] is presenting similar approach to [21] based on solution of algebraic equations. However this method is only testing a collision and it is not interested in minimum distance calculation. Moser introduces two algorithms for intersection calculation. The first one is based on roots estimation and the second one is using gradient approach, which is identified later on.

Eberly defines an ellipsoid E_i by the quadratic equation

$$Q_i(\boldsymbol{X}) = \boldsymbol{X}^T \boldsymbol{A}_i X + \boldsymbol{X}^T \boldsymbol{B}_i + C_i \tag{2.1}$$

or

$$Q_i(\boldsymbol{X}) = \begin{bmatrix} x & y & z \end{bmatrix} \begin{bmatrix} a^i_{00} & a^i_{01} & a^i_{02} \\ a^i_{10} & a^i_{11} & a^i_{12} \\ a^i_{20} & a^i_{21} & a^i_{22} \end{bmatrix} \begin{bmatrix} x \\ y \\ z \end{bmatrix} + \begin{bmatrix} b^i_0 & b^i_1 & b^i_2 \end{bmatrix} \begin{bmatrix} x \\ y \\ z \end{bmatrix} + c^i, \text{ for} i \in \{1, 2\}. \tag{2.2}$$

Whilst $\boldsymbol{Q}_i(\boldsymbol{X}) < 0$ defines interior of the ellipsoid, $\boldsymbol{Q}_i(\boldsymbol{X}] > 0$ defines the exterior. It is obvious that $\boldsymbol{Q}_i(\boldsymbol{X} = 0$ express point on the surface.

Roots calculation

Two polynomials $f(z) = \alpha_0 + \alpha_1 z + \alpha_2 z^2$ and $g(z) = \beta_0 + \beta_1 z + \beta_2 z^2$ have a common root if and only if the Bézout determinant is equal to zero, namely

$$(\alpha_2\beta_1 - \alpha_1\beta_2)(\alpha_1\beta_0 - \alpha_0\beta_1) - (\alpha_2\beta_0 - \alpha_0\beta_2)^2 = 0. \tag{2.3}$$

When the Bézout determinant is equal to zero, a common roots of $f(z)$ and $g(z)$ are

$$\tilde{z} = \frac{\alpha_2\beta_0 - \alpha_0\beta_2}{\alpha_1\beta_2 - \alpha_2\beta_1}. \tag{2.4}$$

Ellipsoid equation may be written to be a quadratic in z, whose coefficients are polynomial in the way of x and y as

$$\begin{aligned} Q_I(x,y,z) = &\left(a^i_{00}x^2 + 2a^i_{01}xy + a^i_{11}y + b^i_0 x + b^i_1 y + c^i\right) + \\ &+ \left(2a^i_{02}x + 2a^i_{12}y + b^i_2\right) z + a^i_{22}z^2. \end{aligned} \tag{2.5}$$

Using the algorithm mentioned above, one can get a polynomial of degree 16 and can find the particular roots. The main disadvantage of this approach is that calculation of the the roots may cause ill-conditioned problem.

Gradient approach

Alternative solution is to set up a system of differential equations, which is walking along one ellipsoid and is searching the point of intersection with the second one. The method results in finding the particular point or evaluate that there is no such points.

One starts with point $\boldsymbol{X}_0$ such as that $Q_0(\boldsymbol{X}_0) = 0$. It concerns any point placed on the surface. The first step is testing if $Q_1(\boldsymbol{X}_0) = 0$. If so, contact point was directly found. This condition means that the particular point is on the surface of both ellipsoids. If $Q_1(\boldsymbol{X}_0) < 0$ the point $\boldsymbol{X}_0$ lies inside and if $Q_1(\boldsymbol{X}_0) > 0$, it lies outside the second ellipsoid respectively. The main idea is to follow the direction of tangential of the first surface in such a way to reach value of $Q_1 = 0$. The best and fastest approach provides the direction of gradient Q_1. Once the point $\boldsymbol{X}_n$ is found, for which $Q_1(\boldsymbol{X}_n) = 0$, the point distance method can be applied. For detailed description see [2].

Analytical solution

Rob [19] defines minimum distance between line

$$y = kx + q \tag{2.6}$$

and ellipse

$$Ax^2 + By^2 = C. \tag{2.7}$$

The points where the extrema are located are points where the tangent to the ellipse is parallel to the line. The slope of the line is k, so the task is to find the points where the tangent has slope k. Doing this by using implicit differentiation on the equation of the ellipse, one gets

$$2Ax + 2By\frac{\partial y}{\partial x} = 0 \tag{2.8}$$

$$\frac{\partial y}{\partial x} = -\frac{Ax}{By} \tag{2.9}$$

$$-\frac{Ax}{By} = k \tag{2.10}$$

$$x = \frac{Bky}{A}. \tag{2.11}$$

The extrema both lie on this line and the ellipse, so finding their intersection will give us the extrema. One will be a maximum and one a minimum, so the minimum distance d of a point $[x_0, y_0]$ from the line 2.6 is

$$d = \min\left\{\frac{|kx_0 - y_0 + q|}{\sqrt{k^2 + 1}}\right\}. \tag{2.12}$$

2.3 Contact force models

The purpose of this section is to provide an overview of impact and contact model methodologies. Energy absorbing, behaviour of a friction model, solution approach, multi-contact problem and experimental testing verification are some of aspects, which are taken into account. Here, it brings a review of results already presented in literature describing the existing models, their relationships other and applications of these impact (contact) models.

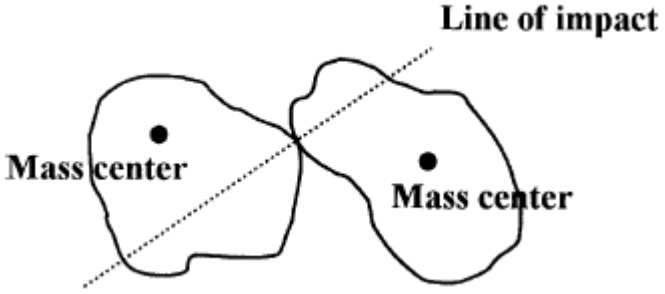

Figure 2.3: Impact of two bodies [3]

In general, two different approaches for contact analysis can be distinguished, namely the discrete and continuous contact model. This text describes both, including unilateral constrain approach, that is generalization of discrete model for multi-contact problem.

2.3.1 Discrete contact model

The discrete contact model formulation is based on the assumption that the impact process is instantaneous, impact forces are impulsive kinetic variables having discontinuous changes, while no displacements occur during the impact and other forces are neglectible. This models are usually used for rigid or very hard bodies, whilst the effects of deformation at the contact point are taking into account through coefficients. The impact problem is then solved by the linear and angular impulse-momentum characteristics between the variables before and after the impact using the coefficient of restitution.

Classical impact theory

Let us assume the planar impact of two bodies with masses m_i, $i \in \{1, 2\}$ and initial velocities v_{i0}, $i \in \{1, 2\}$ and let us divide the impact process into 2 phases, see Fig. 2.4. Consequently loading in $t \in [t_1, t_2]$ is characterized by the linear impulse P_1 and unloading during $t \in (t_2, t_3]$ is characterized by the linear impulse P_2 as

$$P_2 = \epsilon P_1, \tag{2.13}$$

where the coefficient of restitution $\epsilon \in \{0, 1\}$ describes the local changes and

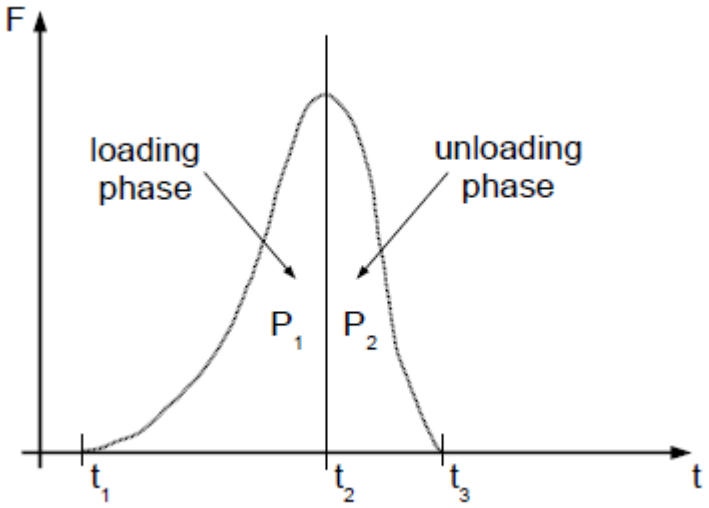

Figure 2.4: Loading and unloading phases of discrete contact model

$$P_1 = \int_{t_1}^{t_2} F dt, \tag{2.14}$$

is the impulse caused by the one dimensional impact, see Fig. 2.4. Here $t \in [t_0, t_2]$ is the impact interval. Whilst $\epsilon = 1$ means completely plastic impact, $\epsilon = 0$ means completely elastic impact.

Linear and angular velocities of particular bodies can be defined [3] as

$$\begin{aligned} v_1 &= v_{10} - (1+\epsilon)\tfrac{P_1}{m_1}\,, \\ v_2 &= v_{20} + (1+\epsilon)\tfrac{P_1}{m_2}\,, \\ \omega_1 &= \omega_{10} - (1+\epsilon) r_{S1}\tfrac{P_1}{I_{S1}}\,, \\ \omega_2 &= \omega_{20} + (1+\epsilon) r_{S2}\tfrac{P_1}{I_{S2}}. \end{aligned} \tag{2.15}$$

Equations (2.15) can be simply solved for impacts between 2 bodies. However, system with more bodies together is complicated to be handled because each impact state influence the remaining system kinematics. Furthermore, the problems involving multiple impacts should be managed as a complex system for better algorithm development and programming.

Coefficient of restitution models

Let have the triad vector (**n**, **t**, **b**) defining a coordinate system with origin at the contact point where **n** is the normal vector to body at this point and vectors **t** **b** define tangent plain (obviously perpendicular to **n**). The total linear impulse can be written as

$$\boldsymbol{P} = P_n\boldsymbol{n} + P_t\boldsymbol{t} + P_b\boldsymbol{b}. \tag{2.16}$$

The relative linear velocity at the contact point has following components: compression velocity along normal direction and component velocity along **t** and **b** direction called sliding velocity. Main variations of the restitution models are reported.

Poisson's model

The total normal impulse P_f is divided into two parts, P_c and P_r, corresponding to compression and restitution phases, respectively. Coefficient of restitution is than defined as

$$\epsilon = \frac{P_r}{P_c}, \quad P_f = P_c + P_r. \tag{2.17}$$

The condition for the end of compression phase is expressed by relative velocity along the normal direction equal to zero.

Newton's model

The coefficient of restitution here is

$$\epsilon = \frac{\boldsymbol{C}(t_f)\ \mathbf{n}}{\boldsymbol{C}(t_0)\ \mathbf{n}} = -\frac{C_f}{C_0}. \tag{2.18}$$

This model is based on kinematic point of view and only the initial and final conditions for the relative normal velocity are taken into account.

Stronge's model

This model is based on the internal energy dissipation hypothesis. The coefficient of restitution is defined as the square root of the ratio of energy released during restitution to the energy absorbed during compression phase. In the terms of work done by the normal force during compression and restitution phases, the coefficient or restitution can be calculated from

$$\epsilon^2 = \frac{W_r}{-W_c}. \tag{2.19}$$

Unilateral constraints approach

The unilateral constraints approach is based on the discrete impact model but it overcomes the problem by defining multiple impact. The multiple contact includes a combinatorial problem of a large dimension. If one contact changes, all other contacts are influenced and it makes a new set of contact configurations necessary to be analysed [15]. Hence it makes sense to define the sets

$$\begin{array}{rcll} I_S & = & \{1,\ldots,m\}, & \text{with } m \text{ contact point,} \\ I_C(t) & = & \{j \in I_S(t) \,:\, \Phi_{N_j} = 0\}, & \text{with } m_C \text{ elements,} \\ I_N(t) & = & \{j \in I_C(t) \,:\, \dot{\Phi}_{N_j} = 0\}, & \text{with } m_N \text{elements,} \\ I_T(t) & = & \{j \in I_T(t) \,:\, |\dot{\Phi}_{T_j}| = 0\}, & \text{with } m_T \text{ elements} \end{array} \tag{2.20}$$

where I_S is the set of all contact points, I_C contains the constraints with vanishing distance with arbitrary relative velocity, I_N describe the constraints fullfiling the necessary conditions for continuous contact (vanishing distance at zero relative velocity in the normal direction) and I_T are the possibly sticking contacts. Φ_j and $\dot{\Phi}_j$ are the relative distances and velocities between the contacting bodies for the j-th contact and indices N and T mark normal and tangential directions respectively. Since each contact event change influences all other contact events in the multibody system, these sets depend on time t. The transition between one state to another one are governed by complementaries in normal and tangential directions defining the corresponding unilateral constrains [16].

Due to the complication using the discrete contact modelling approach (timing in multiple contact using classical impact theory or computationally expensive quadratic programming programming using unilateral constraints approach), the following approach assuming contact force as the external force dependent on the local indentation between the impacting bodies is usually used.

2.3.2 Continuous contact model

The continuous contact model is useful to overcome the problem with local deformation, non-smoothness in contact variables and energy absorption that is complicated to be described by the discrete contact models. The basic of the continuous model formulation for contact dynamics is in an explicitly account of the deformation of the bodies during impact (contact). In a large class of continuous models is defined by applying by defining the normal contact force F_n as an explicit function of a local indentation δ as

$$F_n \equiv F_n(\dot{\delta}, \delta). \tag{2.21}$$

The dependence of force on indentation is a crucial relation which has to be known or otherwise unrealistic situations might appear. In the following text, a summary of the three existing contact force models are analysed.

Hertz's model

Hertz's model [3, 9] is non-linear and it does not include any damping. However, it is limited only to an impact of elastic deformation. Hertz's model contact problem can be constructed as interaction of two rigid bodies via a non-linear spring along the line of impact. The hypothesis is based on assumption, that the deformation is concentrated in the vicinity of the contact point (area). The elastic wave motion is not relevant and the total mass of each body is moving with the velocity of its centre of gravity. The impact force is then defined as

$$F_n = k\delta^n, \tag{2.22}$$

where k and n are constant parameters depending on material and geometric properties of bodies and can be calculated using elastostatic theory [1, 13]. Constant k represents the stiffness parameter. For example, in case of two spheres impact, the value $n = \frac{3}{2}$ and k is varying with Poisson's ratios, Young's moduli and radii of the spheres as

$$k = \frac{4}{3(\sigma_i + \sigma_j)} \left[\frac{R_i R_j}{R_i + R_j} \right], \tag{2.23}$$

where material parameters σ_i and σ_j are defined by

$$\sigma_l = \frac{1-\nu_l^2}{E_l},\ l \in \{i,j\}, \tag{2.24}$$

in which quantities ν_l and E_l are Possion's ratio and Young's modulus associated with particular sphere, respectively.

Since the Hertz's model does not take energy dissipation into account, the coefficient of restitution is equal to one. Gillardi [3] discussed this model is suitable especially for low impact speeds within hard materials. Elastic contact law of the Hertz's model can be upgraded by adding plastic deformation. This can be accomplished by using hysteresis force law, which takes the form

$$F_n = F_{n,max}(\frac{\delta-\delta_p}{\delta_{max}-\delta_p})^n \tag{2.25}$$

where $F_{n,max}$ and δ_{max} are maximum normal force and maximum indentation during loading phases of impact, respectively, and δ_p is permanent indentation. Note that maximum values in the (2.25) is calculated in every instance of numerical solution, value δ is calculated in each time step, but δ_p is an additional parameter, and it has to be defined initially in particular contact model. Hysteresis model is not very common to use since being large, heavy or not effective.

Spring-dashpot model

An alternative contact force model taking account energy loss during impact is a spring-dashpot, or so called Kelvin-Voigt model [3, 9]. The impact is schematically represented with a linear damper (dashpot) for dissipation of energy parallel with linear spring for the elastic behaviour. The normal contact force is defined as

$$F_n = k\delta + b\dot{\delta} \tag{2.26}$$

and an equivalent system to the model is schematically represent in Fig. 2.5.

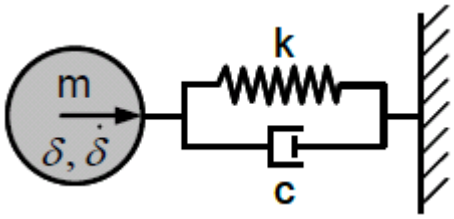

Figure 2.5: Equivalent system [9]

Quantities b and k in Eg. 2.26 represent parameters depending on material and shape of the contacting bodies. δ is indentation (or penetration) and $\dot{\delta}$ is relative normal contact velocity. In some literature [3, 9] $\dot{\delta}$ is defined as a *indentation velocity*.

Three weaknesses of this model are pointed out:

- At the beginning of impact, contact force is discontinuous, because of the damping term. During the real contact situation, both elastic and damping forces should be initially equal ta zero and are increasing over the time.
- When the objects are separating, the indention tends to zero and hence their relative velocity tends to be negative. The results is a negative normal force holding the objects together, is shown in Fig. 2.6.
- The coefficient of restitution for this model does not depend on the impact velocity. Note that velocity dependence of ϵ has to be developed experimentally.

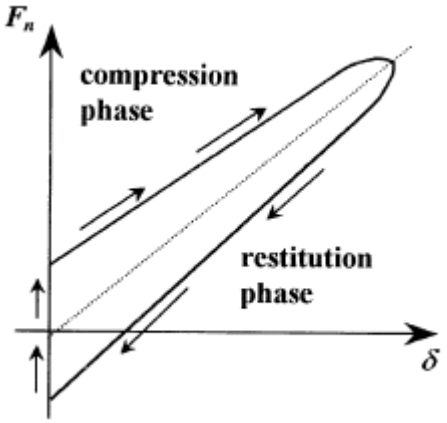

Figure 2.6: Contact force history for the spring-dashpot model [3]

Even the spring-dashpot model is not physically realistic, it is used very often because of its simplicity. It provides a reasonable method to capture energy dissipation effect without explicitly considering plastic deformation issues.

Non-linear damping

Dealing with problems of the spring-dashpot model and retaining the advantages of the Hertz's model, another model involved energy dissipation effect was introduced by Hunt and Crossley [7, 3, 9]. The non-linear damping term is considered and the term of the impact force comes to

$$F_n = k\delta^n + \chi\delta^p\dot{\delta}^q, \tag{2.27}$$

where p, q and n are constants and it is common to set them $p = n$ and $q = 1$. The damping parameter χ is related to the coefficient of restitution, because it is associated with energy dissipation phenomena, similarly with dashpot model.

Based on the literature review and the physical effect, parameter χ is called the hysteresis damping factor and is given by

$$\chi = \frac{3k(1-c_r)}{2\dot{\delta}^{(-)}}, \tag{2.28}$$

in which k represents the generalized stiffness parameter, c_r is the coefficient of restitution and $\dot{\delta}^{(-)}$ is the initial contact velocity. Advantages of this particular model can be described as follows:

- Damping coefficient depends on indentation value, which sound physically realistic.
- There is no discontinuities at initial contact region and separation; it begins and finishes with correct value equal to zero.

Friction model

Coulomb's (discrete) contact law [3] is frequently used to describe an effect of friction in impact. Main disadvantages of the Coulomb's law is the discontinuity of the friction force. To sort this out and to capture effect due to friction interaction, alternative friction force law has been established [3, 9]. The first improvement of the law is obtained by using a non-local friction model where value of friction at one point depends on quantities at numbers of its neighbourhoods. Another improvement is in applying non-linear model to allow a continuous transition from sticking to sliding phases. The friction model is defined as

$$\boldsymbol{F}_t = k_f \boldsymbol{s},\ \boldsymbol{s}(t) = \begin{cases} \boldsymbol{s}(t_0) + \displaystyle\int_{t_0}^{t} \boldsymbol{v}_t dt, & \text{if } |\boldsymbol{s}| < s_{max} \\ s_{max}\dfrac{\boldsymbol{v}_t}{|\boldsymbol{v}_t|}, & \text{otherwise, } s_{max} = |\mu|\dfrac{F_n}{k_f}\ (,) \end{cases} \tag{2.29}$$

where k_f is friction stiffness, $\mathbf{s}$ is the vector of friction displacement, t_0 is the start time of the last sticking at the particular contact point, $\mathbf{v}_t$ is the relative tangential velocity and s_{max} is the parameter of maximum allowable deflection. Very important aspect of this model is the effective calculation of friction force to be a function of time.

Another model, but is is not common to present it as a friction model, is the Stronge's model [3]. This model is using concept of tangential friction force, in the way of the Hertz's model, thus the tangential force is defined as

$$F_t = k_t \delta_t \tag{2.30}$$

where δ_t is tangential component of indentation at the contact point and k_t is tangential stiffness.

Modern methods of friction model appear, coming with a large number of parameters, which is necessary to solve the problem. It is not very straightforward to understand the physical meaning of all the parameters.

Chapter 3

Method

3.1 Double pendulum model

3.1.1 Local and global coordinate systems

Let us consider an arbitrary body located in N-dimensional space. Position of the body and all the points of the body are defined by coordinates $X_i,\ i \in \{1, 2...N\}$. This body can move with a translational motion in the direction of coordinate axes and/or rotational motion around these axes.

During the translational motion all the points on the body are moving in the same direction. Regarding this fact, it is possible to analyse the motion only with one point. It has proved to be a useful choice to set a centre of gravity (later referred as COG) to become this particular point.

During the rotational motion the body is rotating around an axis. Obviously there are not only these simple motions, the body can move in highly complicated manner. However, every real movement, no matter how complex it is, can be decomposed to a series of independent simple motions (translations and rotations).

The final position of the body, which takes place after several simultaneous movements, can be determined from the principle of the independence of movements, or also called the principle of superposition of movements.

Local and global coordinate systems are defined, see Fig. 3.1. Whilst the global coordinate system is time invariant and fixed to the frame, the local one is fixed to the body with origin located at COG.

The general relation between the local and global coordinate systems at any point i on the body is

$$\mathbf{r}^i_{gl} = \mathbf{r}_c + \mathbf{T}\ \mathbf{r}^i_{loc} \tag{3.1}$$

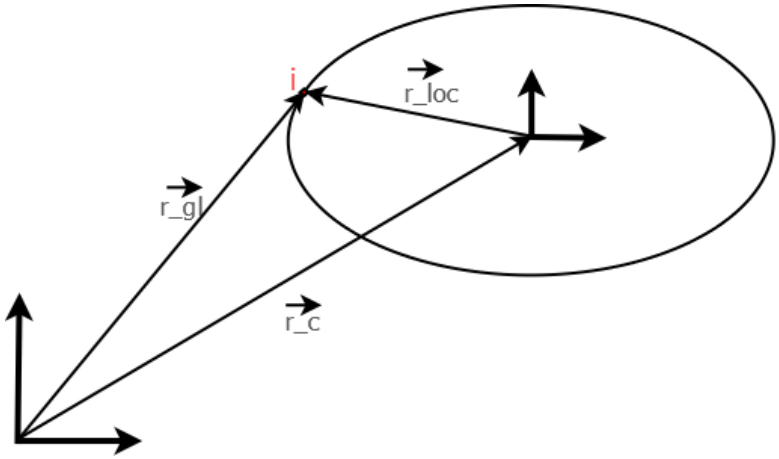

Figure 3.1: Local and global coordinate systems

where $\mathbf{r}^i_{gl}$ represents the global coordinates of point i, $\mathbf{r}_c$ are the coordinates of COG, T denotes transformation matrix between local and global systems and $\mathbf{r}^i_{loc}$ are coordinates of point i in the local coordinate system, see Fig. 3.1.

3.1.2 Spatial motion implementation

The double pendulum is assumed to be composed by two ellipsoids constrained together. Both ellipsoids have major axes a_{ij}, mass m_i and moments of inertia I_{ij}, i $\in \{1, 2\}$ and j $\in \{1, 2, 3\}$. The global coordinate system $\boldsymbol{X}_1 = [x_1, y_1, z_1]$ is defined to be a Cartesian coordinate system with an origin at frame fixed point of the first pendulum (joint) at $[0, 0, 0]^T$ in the global coordinate system. The two bodies are jointed in one point with a spherical kinematic joint as shown in Fig. 3.2.

Let us consider motion of double pendulum to be a motion of two independent bodies, constrained with a mathematical constraint defined later. This assumption is highly important in the methods applied in the mathematical model, respectively in the derivation of equations of motion.

Spherical joint

Any general joint has 6 degrees of freedom (further referred as DOF), namely three translations and three rotations. All of them can be potentially free or fixed. Spherical joint is a type of primitive kinematic constraint with three rotational degree of freedom.

Schematic representation of the bodies i and j constrained together is shown in Fig. 3.3. The point, where body i and j are joined is marked as P. Position of the P point can be defined by the two vectors $\vec{S}^P_i$ in local coordinates system (ξ_1, η_1, ζ_1) of body i and $\vec{S}^P_j$ in coordinates system (ξ_2, η_2, ζ_2) of body j.

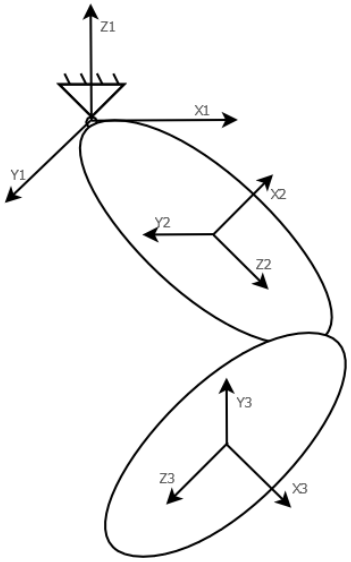

Figure 3.2: Double pendulum

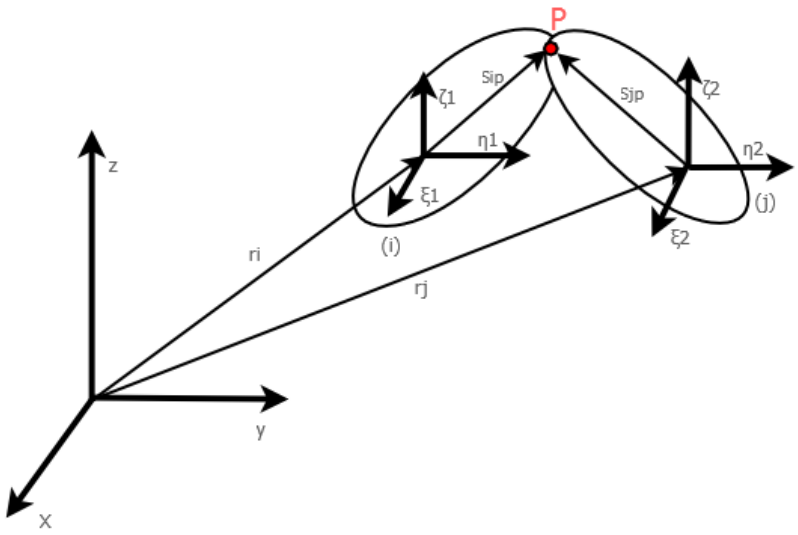

Figure 3.3: Spherical joint

Spherical motion can be considered by three independent rotations, namely precession around the z axis represented with angle ψ, nutation around the "new" x axis represented with ν and rotation around the "actual" z axis represented by angle φ.

The three independent spacial motions can be described by transformation matrices as

$$\mathbf{T}_{pre}(\psi) = \begin{bmatrix} \cos(\psi) & -\sin(\psi) & 0 \\ \sin(\psi) & \cos(\psi) & 0 \\ 0 & 0 & 1 \end{bmatrix}, \tag{3.2}$$

$$\mathbf{T}_{nut}(\nu) = \begin{bmatrix} 1 & 0 & 0 \\ 0 & \cos(\nu) & -\sin(\nu) \\ 0 & \sin(\nu) & \cos(\nu) \end{bmatrix}, \tag{3.3}$$

$$\mathbf{T}_{rot}(\varphi) = \begin{bmatrix} \cos(\varphi) & -\sin(\varphi) & 0 \\ \sin(\varphi) & \cos(\varphi) & 0 \\ 0 & 0 & 1 \end{bmatrix}. \tag{3.4}$$

Regarding Eq. 3.1, the transformation formula in case of spherical movement can be written using translation of centre of gravity and multiplication of precession, nutation and rotation matrices. Thus general transformation of any point of body from local to global coordinate system is described as

$$\boldsymbol{X}_1 = \boldsymbol{X_s} + \boldsymbol{T}_{pre}(\psi)\ \boldsymbol{T}_{nut}(\nu)\ \boldsymbol{T}_{rot}(\varphi)\ \boldsymbol{X}_2 \tag{3.5}$$

where $T_i, i \in \{1, 2, 3\}$ are transformation matrices of precession, nutation and rotation respectively. Eq. 3.5 can be rewritten using only one transformation matrix

$$\boldsymbol{X}_1 = \boldsymbol{X}_s + \boldsymbol{T}_{12}\ \boldsymbol{X}_2 \tag{3.6}$$

where $\boldsymbol{T}_{12}$ is a transformation matrix between the local coordinate body-fixed system 2 to the global coordinate system 1 and $\boldsymbol{X}_s$ represents coordinates of COG.

Transformation matrix $\boldsymbol{T}_{12}$ is a three dimensional matrix generated by multiplying of $\boldsymbol{T}_{pre}$, $\boldsymbol{T}_{nut}$ and $\boldsymbol{T}_{rot}$, thus

$$\boldsymbol{T}_{12}(\psi, \nu, \varphi) =$$

$$\begin{bmatrix} \cos(\varphi)\cos(\psi) - \cos(\nu)\sin(\varphi)\sin(\psi) & -\cos(\psi)\sin(\varphi) - \cos(\varphi)\cos(\nu)\sin(\psi) & \sin(\nu)\sin(\psi) \\ \cos(\varphi)\sin(\psi) + \cos(\nu)\cos(\psi)\sin(\varphi) & \cos(\varphi)\cos(\nu)\cos(\psi) - \sin(\varphi)\sin(\psi) & -\cos(\psi)\sin(\nu) \\ \sin(\varphi)\sin(\nu) & \cos(\varphi)\sin(\nu) & \cos(\nu) \end{bmatrix} \tag{3.7}$$

Double pendulum coordinates

Since the motion of double pendulum is considered to be a translation of centre of gravity and spherical rotation around this point, the transformation defined above can be applied in order to describe the system. Taking into account Eq. 3.6, position of any arbitrary point at body 1 and 2 in global coordinates system can be define as

$$\mathbf{X}_1 = \mathbf{X}_{si} + \mathbf{T}_{1i}(\psi_j, \nu_j, \varphi_j)\ \mathbf{X}_i, \text{ where i} \in \{2, 3\}. \tag{3.8}$$

Thus:

- The first body global coordinates: $i = 2$

$$\mathbf{X}_1 = \mathbf{X}_{s2} + \mathbf{T}_{12}(\psi_2, \nu_2, \varphi_2)\ \mathbf{X}_2 \tag{3.9}$$

- The second body global coordinates: $i = 3$

$$\mathbf{X}_1 = \mathbf{X}_{s3} + \mathbf{T}_{13}(\psi_3, \nu_3, \varphi_3), \mathbf{X}_3 \tag{3.10}$$

where $\boldsymbol{X}_{s2}$ represents the first body COG coordinates and $\boldsymbol{X}_2$ is the coordinates vector of any particular point in the local coordinate system of the first body. $\mathbf{X}_{s3}$ is the vector of COG coordinates of the second body and $\boldsymbol{X}_3$ are coordinates of any arbitrary point in the local coordinate system of the second body. Note that matrices T_{12} and T_{13} are formally identical, the only difference is that T_{12} is a function of angles $(\psi_2, \nu_2, \varphi_2)$ and T_{13} is function of angles $(\psi_3, \nu_3, \varphi_3)$. These variables are known as the Euler's angles [14].

Finally, the vector of generalized coordinates of the system can be defined. Generalized coordinates of the system with n DOF are q_i where $i \in \{1, 2...m\}$ and $m \geq n$. In this case, the generalized coordinates vector is

$$\boldsymbol{q} = [x_{s2}, y_{s2}, z_{s2}, \psi_2, \nu_2, \varphi_2, x_{s3}, y_{s3}, z_{s3}, \psi_3, \nu_3, \varphi_3]^T.$$

3.1.3 Equation of motion

Equations of motion (later referred as EOM) are derived from the Lagrange's equations of a second kind, which incorporates the constraints directly by means of generalized coordinates.

General formula for the Lagrange's equation of second kind is

$$\frac{d}{dt}\frac{\partial L}{\partial \dot{\boldsymbol{q}}} - \frac{\partial L}{\partial \boldsymbol{q}} = \boldsymbol{Q} + \sum_{j=1}^{r} \lambda_j \frac{\partial \Phi_j}{\partial \boldsymbol{q}}, \tag{3.11}$$

where $L = E_k - E_p$ is called Lagrangian, $\boldsymbol{Q}$ represents generalized forces, λ are the Lagrange's multipliers and Φ_j are the constraint equations.

Since E_k is not function of $\dot{q}_i$ and E_p is only function of q_i in the double pendulum system (here $i \in \{1 \dots 12\}$ and $r = 6$), Eq. 3.11 can be rewritten as

$$\frac{d}{dt}\frac{\partial E_k}{\partial \dot{q}_i} - \frac{\partial E_p}{\partial q_i} = Q_i + \sum_{j=1}^{6} \lambda_j \frac{\partial \Phi_j}{\partial q_i} \tag{3.12}$$

where E_k and E_p are kinetic and potential energy, respectively.

Energy balance

Kinetic energy of the system following the König's rule and the assumption of two independent bodies expressed in global coordinates is

$$E_k = \frac{1}{2}\sum \dot{\boldsymbol{X}}_s^T \tilde{\boldsymbol{M}}_i \dot{\boldsymbol{X}}_{si} + \frac{1}{2}\sum \boldsymbol{\omega_i^T} \tilde{\boldsymbol{I}}_i \boldsymbol{\omega_i} = \frac{1}{2}\sum \dot{\boldsymbol{q}}^T \boldsymbol{M} \dot{\boldsymbol{q}}. \tag{3.13}$$

Potential energy of the system is

$$E_p = \sum_{l=1}^{2} m_l g z_{sl}. \tag{3.14}$$

Derivatives of kinetic energy with respect to generalized velocities (derivation of generalized coordinates) are

$$\frac{\partial E_k}{\partial \dot{q}_i} = \boldsymbol{M}\dot{\boldsymbol{q}}. \tag{3.15}$$

Derivatives of Eq. 3.15 with respect to time place the form

$$\frac{d}{dt}\frac{\partial E_k}{\partial \dot{q}_i} = \boldsymbol{M}\ddot{\boldsymbol{q}}, \tag{3.16}$$

where $\boldsymbol{q}$ is generalized coordinates vector and $\boldsymbol{M}$ is a mass matrix

$$\boldsymbol{M} = \begin{bmatrix} \mathrm{m}_1 & 0 & 0 & 0 & 0 & 0 & 0 & 0 & 0 & 0 & 0 & 0 \\ 0 & \mathrm{m}_1 & 0 & 0 & 0 & 0 & 0 & 0 & 0 & 0 & 0 & 0 \\ 0 & 0 & \mathrm{m}_1 & 0 & 0 & 0 & 0 & 0 & 0 & 0 & 0 & 0 \\ 0 & 0 & 0 & \mathrm{I}_{11} & 0 & 0 & 0 & 0 & 0 & 0 & 0 & 0 \\ 0 & 0 & 0 & 0 & \mathrm{I}_{12} & 0 & 0 & 0 & 0 & 0 & 0 & 0 \\ 0 & 0 & 0 & 0 & 0 & \mathrm{I}_{13} & 0 & 0 & 0 & 0 & 0 & 0 \\ 0 & 0 & 0 & 0 & 0 & 0 & \mathrm{m}_2 & 0 & 0 & 0 & 0 & 0 \\ 0 & 0 & 0 & 0 & 0 & 0 & 0 & \mathrm{m}_2 & 0 & 0 & 0 & 0 \\ 0 & 0 & 0 & 0 & 0 & 0 & 0 & 0 & \mathrm{m}_2 & 0 & 0 & 0 \\ 0 & 0 & 0 & 0 & 0 & 0 & 0 & 0 & 0 & \mathrm{I}_{21} & 0 & 0 \\ 0 & 0 & 0 & 0 & 0 & 0 & 0 & 0 & 0 & 0 & \mathrm{I}_{22} & 0 \\ 0 & 0 & 0 & 0 & 0 & 0 & 0 & 0 & 0 & 0 & 0 & \mathrm{I}_{23} \end{bmatrix}. \tag{3.17}$$

Non-zero derivatives of potential energy with respect to generalized coordinates are

$$\frac{\partial E_p}{\partial q_i} = m_i g, \ i \in \{3, 9\}. \tag{3.18}$$

Note that

$$\frac{\partial E_p}{\partial q_i} = 0 \ i \in \{1, 2, 4, 5, 6, 7, 8, 10, 11, 12\}. \tag{3.19}$$

3.1.4 Kinematics constrains definition

Kinematic constrain equations defined in Eq. 3.12 are developed in this paragraph. The set of kinematic constraints need to be expressed and added to the system.

Spherical joint fixation of the upper peak of the first body that concerns the zero displacement of the point $\boldsymbol{X}_2$). By meaning of Eq. 3.6, the first constraint equation can be written. The local coordinates of $\boldsymbol{X}_2$ are $x_2 = 0$, $y_2 = 0$ and $z_2 = -a_{13}$, hence the vector is $\boldsymbol{X}_2 = [0, 0, -a_{13}]^T$ and the constraint equation is

$$\boldsymbol{\Phi}_1 = \boldsymbol{X}_{s2} + \boldsymbol{T}_{12} \begin{bmatrix} 0 \\ 0 \\ -a_{13} \end{bmatrix} = \begin{bmatrix} 0 \\ 0 \\ 0 \end{bmatrix}. \tag{3.20}$$

Link between the top (upper) peak of the second body and the bottom peak of the first body that means the two points are coincident all over the time. These points are $[0, 0, a_{13}]^T$ in the local coordinate system of first body, and $[0, 0, -a_{23}]^T$ in the local coordinate system of the second body.

Thus using equations 3.9 and 3.10), the first constraint equation is

$$\boldsymbol{X}_{s2} + \boldsymbol{T}_{12} \begin{bmatrix} 0 \\ 0 \\ a_{13} \end{bmatrix} = \boldsymbol{X}_{s3} + \boldsymbol{T}_{13} \begin{bmatrix} 0 \\ 0 \\ -a_{23} \end{bmatrix} \tag{3.21}$$

and thus second constrain equation is

$$\boldsymbol{\Phi}_2 = \boldsymbol{X}_{s2} + \boldsymbol{T}_{12} \begin{bmatrix} 0 \\ 0 \\ a_{13} \end{bmatrix} - \boldsymbol{X}_{s3} - \mathbf{T}_{13} \begin{bmatrix} 0 \\ 0 \\ -a_{23} \end{bmatrix} = \begin{bmatrix} 0 \\ 0 \\ 0 \end{bmatrix}. \tag{3.22}$$

Both constrain equations 3.21 and 3.22 together can be written in a compact matrix form as

$$\boldsymbol{\Phi} = \begin{bmatrix} \boldsymbol{\Phi}_1 \\ \boldsymbol{\Phi}_2 \end{bmatrix} = \begin{bmatrix} \Phi_1 \\ \Phi_2 \\ \Phi_3 \\ \Phi_4 \\ \Phi_5 \\ \Phi_6 \end{bmatrix} = \begin{bmatrix} \boldsymbol{X}_{s2} + \boldsymbol{T}_{12} \begin{bmatrix} 0 \\ 0 \\ -a_{13} \end{bmatrix} \\ \boldsymbol{X}_{s2} + \boldsymbol{T}_{12} \begin{bmatrix} 0 \\ 0 \\ a_{13} \end{bmatrix} - \boldsymbol{X}_{s3} - \boldsymbol{T}_{13} \begin{bmatrix} 0 \\ 0 \\ -a_{23} \end{bmatrix} \end{bmatrix} = \begin{bmatrix} 0 \\ 0 \\ 0 \\ 0 \\ 0 \\ 0 \end{bmatrix}. \tag{3.23}$$

This generates six equations for the constrains

$$\boldsymbol{\Phi}(\boldsymbol{q}(t)) = \begin{bmatrix} \mathrm{x_{s2}} - \mathrm{a_{13}}\ \sin(\nu_2)\ \sin(\psi_2) \\ \mathrm{y_{s2}} + \mathrm{a_{13}}\ \cos(\psi_2)\ \sin(\nu_2) \\ \mathrm{z_{s2}} - \mathrm{a_{13}}\ \cos(\nu_2) \\ \mathrm{x_{s2}} - \mathrm{x_{s3}} + \mathrm{a_{13}}\ \sin(\nu_2)\ \sin(\psi_2) + \mathrm{a_{23}}\ \sin(\nu_3)\ \sin(\psi_3) \\ \mathrm{y_{s2}} - \mathrm{y_{s3}} - \mathrm{a_{13}}\ \cos(\psi_2)\ \sin(\nu_2) - \mathrm{a_{23}}\ \cos(\psi + 3)\ \sin(\nu_3) \\ \mathrm{z_{s2}} - \mathrm{z_{s3}} + \mathrm{a_{13}}\ \cos(\nu_2) + \mathrm{a_{23}}\ \cos(\nu_3) \end{bmatrix} = \mathbf{0}. \tag{3.24}$$

The constrained system hence has 6 degrees of freedom in total.

Second derivatives of constrain

Regarding the Lagrange's equations of the second kind, to derive equations of motion, the second derivatives of constrains Eq. 3.24 with respect of time need to be obtained and added to system Eq. 3.12.

Vector $\boldsymbol{\Phi}$ is a vector of six independent constraint equations, which are functions of generalized coordinates and also function of time.

Thus, the first derivatives with respecting to time generate vector

$$\frac{d\boldsymbol{\Phi}}{dt} \equiv \dot{\boldsymbol{\Phi}} = \left[\frac{\partial \boldsymbol{\Phi}}{\partial x_{s2}} \dot{x}_{s2} + \frac{\partial \boldsymbol{\Phi}}{\partial y_{s2}} \dot{y}_{s2} + \frac{\partial \boldsymbol{\Phi}}{\partial z_{s2}} \dot{z}_{s2} + \ldots \qquad \ldots + \frac{\partial \boldsymbol{\Phi}}{\partial \nu_3} \dot{\nu}_3 + \frac{\partial \boldsymbol{\Phi}}{\partial \varphi_3} \dot{\varphi}_3 \right] \tag{3.25}$$

that can be simply written as

$$\dot{\mathbf{\Phi}} = \sum_{i=1}^{12} \frac{\partial \mathbf{\Phi}}{\partial q_i} \dot{q}_i. \tag{3.26}$$

The second time derivatives then takes a form

$$\frac{d\dot{\mathbf{\Phi}}}{dt} \equiv \ddot{\mathbf{\Phi}} = \left[\frac{\partial^2 \mathbf{\Phi}}{\partial x_{s2}^2} \dot{x}_{s2}^2 + \frac{\partial^2 \mathbf{\Phi}}{\partial x_{s2} y_{s2}} \dot{x}_{s2} \dot{y}_{s2} + ... \quad ... + \frac{\partial \mathbf{\Phi}}{\partial x_{s2}} \dot{x}_{s2} + ... \quad ... + \frac{\partial \mathbf{\Phi}}{\partial \varphi_3} \dot{\varphi}_3 \right], \tag{3.27}$$

or

$$\ddot{\mathbf{\Phi}} = \sum_{i=1}^{12} \sum_{j=1}^{12} \frac{\partial^2 \mathbf{\Phi}}{\partial q_i \partial q_j} \dot{q}_i \dot{q}_j. \tag{3.28}$$

Differential-algebraic equation

The EOM derived in the previous paragraph leads to the system of differential-algebraic equation (further referred as DAE). An important quantity characterising DAE is their differential index. It can be defined as a number, how many times the DAE need to be differentiate to reach standard system ordinary differential equations. The higher value of differential index corresponds with more complex and difficult DAE integration.

Eq. 3.12 together with constrain Eq. 3.28 constitute a mathematical model of the constrained multibody system. Formulating EOM using these constrained generalized coordinates leads to the mathematical model in the form of the set of DAE in the form

$$\begin{bmatrix} \mathbf{M} & \mathbf{\Phi}^T \\ \mathbf{\Phi} & \mathbf{0} \end{bmatrix} \cdot \begin{bmatrix} \ddot{\boldsymbol{q}} \\ -\boldsymbol{\lambda} \end{bmatrix} = \begin{bmatrix} \boldsymbol{f}(\boldsymbol{q}, \dot{\boldsymbol{q}}, t) \\ \boldsymbol{\gamma}(\boldsymbol{q}, \dot{\boldsymbol{q}}, t) \end{bmatrix} \tag{3.29}$$

where

$$\mathbf{\Phi} = \begin{bmatrix} 1 & 0 & 0 & -\mathrm{a}_{13}\, c(\psi_2)\ s(\nu_2) & -\mathrm{a}_{13}\, c(\nu_2)\ s(\psi_2) & 0 & 0 & 0 & 0 & 0 & 0 & 0 \\ 0 & 1 & 0 & -\mathrm{a}_{13}\, s(\nu_2)\ s(\psi_2) & \mathrm{a}_{13}\, c(\nu_2)\ c(\psi_2) & 0 & 0 & 0 & 0 & 0 & 0 & 0 \\ 0 & 0 & 1 & 0 & \mathrm{a}_{13}\, s(\nu_2) & 0 & 0 & 0 & 0 & 0 & 0 & 0 \\ 1 & 0 & 0 & \mathrm{a}_{13}\, c(\psi_2)\ s(\nu_2) & \mathrm{a}_{13}\, c(\nu_2)\ s(\psi_2) & 0 & 1 & 0 & 0 & -\mathrm{a}_{23}\, c(\psi_3)\ s(\nu_3) & -\mathrm{a}_{23}\, c(\nu_3)\ s(\psi_3) & 0 \\ 0 & 1 & 0 & \mathrm{a}_{13}\, s(\nu_2)\ s(\psi_2) & -\mathrm{a}_{13}\, c(\nu_2)\ c(\psi_2) & 0 & 0 & 1 & 0 & -\mathrm{a}_{23}\, s(\nu_3)\ s(\psi_3) & \mathrm{a}_{23}\, c(\nu_3)\ c(\psi_3) & 0 \\ 0 & 0 & 1 & 0 & -\mathrm{a}_{13}\, s(\nu_2) & 0 & 0 & 0 & 1 & 0 & \mathrm{a}_{23}\, s(\nu_3) & 0 \end{bmatrix}, \tag{3.30}$$

$$\boldsymbol{f} = \begin{bmatrix} 0 \\ 0 \\ -\mathrm{m}_1\ g \\ 0 \\ 0 \\ 0 \\ 0 \\ 0 \\ -\mathrm{m}_2\ g \\ 0 \\ 0 \\ 0 \end{bmatrix}, \tag{3.31}$$

$$\boldsymbol{\Gamma} =$$

$$\begin{bmatrix} -\mathrm{a}_{13}\, s(\nu_2)\ s(\psi_2)\ \dot{\nu}_2^2 + \mathrm{a}_{13}\, c(\nu_2)\ c(\psi_2)\ \dot{\nu}_2\, \dot{\psi}_2\, 2 - \mathrm{a}_{13}\, s(\nu_2)\ s(\psi_2)\ \dot{\psi}_2^2 \\ \mathrm{a}_{13}\, c(\psi_2)\ s(\nu_2)\ \dot{\nu}_2^2 + \mathrm{a}_{13}\, c(\nu_2)\ s(\psi_2)\ \dot{\nu}_2\, \mathrm{d}\psi_2\, 2 + \mathrm{a}_{13}\, c(\psi_2)\ s(\nu_2)\ \dot{\psi}_2^2 \\ -\mathrm{a}_{13}\, \dot{\nu}_2^2\, c(\nu_2) \\ \mathrm{a}_{13}\, s(\nu_2)\ s(\psi_2)\ \dot{\nu}_2^2 - \mathrm{a}_{13}\, c(\nu_2)\ c(\psi_2)\ \dot{\nu}_2\, \dot{\psi}_2\, 2 - \mathrm{a}_{23}\, s(\nu_3)\ s(\psi_3)\ \dot{\nu}_3^2 + \mathrm{a}_{23}\, c(\nu_3)\ c(\psi_3)\ \dot{\nu}_3\, \dot{\psi}_3\, 2 + \mathrm{a}_{13}\, s(\nu_2)\ s(\psi_2)\ \dot{\psi}_2^2 - \mathrm{a}_{23}\, s(\nu_3)\ s(\psi_3)\ \dot{\psi}_3^2 \\ -\mathrm{a}_{13}\, c(\psi_2)\ s(\nu_2)\ \dot{\nu}_2^2 - \mathrm{a}_{13}\, c(\nu_2)\ s(\psi_2)\ \dot{\nu}_2\, \dot{\psi}_2\, 2 + \mathrm{a}_{23}\, c(\psi_3)\ s(\nu_3)\ \dot{\nu}_3^2 + \mathrm{a}_{23}\, c(\nu_3)\ s(\psi_3)\ \dot{\nu}_3\, \dot{\psi}_3\, 2 - \mathrm{a}_{13}\, c(\psi_2)\ s(\nu_2)\ \dot{\psi}_2^2 + \mathrm{a}_{23}\, c(\psi_3)\ s(\nu_3)\ \dot{\psi}_3^2 \\ \mathrm{a}_{13}\, \dot{\nu}_2^2\, c(\nu_2) - \mathrm{a}_{23}\, \dot{\nu}_3^2\, c(\nu_3) \end{bmatrix} \tag{3.32}$$

where s symbolized *sin* and c is *cos*, respectivelly.

The vector of unknown generalized accelerations (the second derivatives of generalized coordinates with respect to time) is defined as

$$\ddot{\boldsymbol{q}} = \begin{bmatrix} \ddot{\mathrm{x}}_{\mathrm{s}2} \\ \ddot{\mathrm{y}}_{\mathrm{s}2} \\ \ddot{\mathrm{z}}_{\mathrm{s}2} \\ \ddot{\psi}_2 \\ \ddot{\nu}_2 \\ \ddot{\varphi}_2 \\ \ddot{\mathrm{x}}_{\mathrm{s}3} \\ \ddot{\mathrm{y}}_{\mathrm{s}3} \\ \ddot{\mathrm{z}}_{\mathrm{s}3} \\ \ddot{\psi}_3 \\ \ddot{\nu}_3 \\ \ddot{\varphi}_3 \end{bmatrix}. \tag{3.33}$$

The vector of the Lagrange's multipliers, which also represents reaction forces is in form

$$\boldsymbol{\lambda} = \begin{bmatrix} \lambda_1 \\ \lambda_2 \\ \lambda_3 \\ \lambda_4 \\ \lambda_5 \\ \lambda_6 \end{bmatrix}. \tag{3.34}$$

According to [6], Eq. 3.29 is DAE of index one. Another important classification of differential equations is whether it is a stiff or a non-stiff problem, associated with eigen-frequency distribution [6]. This fact causes difficulties during numerical integration, and due to this special numerical solver are implemented.

3.1.5 Numerical solution

Eq. 3.29 represents a system of 18 dependent DAE. One principle to solve this system is in eliminating the Lagrange's multipliers and transforming the second order equations to the system of the first order equations. The particular substitution is then

$$\boldsymbol{v} = \dot{\boldsymbol{q}} \tag{3.35}$$

and

$$\dot{\boldsymbol{v}} = \ddot{\boldsymbol{q}}. \tag{3.36}$$

To express accelerations $\ddot{\boldsymbol{q}}$ and consequence application of numerical integration, the approach based on transformation of DAE into a underlying ODE by method so called elimination of the Lagrange's multipliers. To avoid difficulties with commutating Lagrange multipliers, the accelerations are expressed from Eq. 3.29, which represents two vector equations, as

$$\boldsymbol{M}\ddot{\boldsymbol{q}} - \boldsymbol{\Phi}^{\boldsymbol{T}}\boldsymbol{\lambda} = \boldsymbol{p} \tag{3.37}$$

and

$$\boldsymbol{\Phi}\ddot{\boldsymbol{q}} = \boldsymbol{\gamma}. \tag{3.38}$$

Accelerations are expressed from Eq. 3.37 as

$$\ddot{\boldsymbol{q}} = \boldsymbol{M}^{-1}\left(\boldsymbol{p} + \boldsymbol{\phi}^{\boldsymbol{T}}\boldsymbol{\lambda}\right) \tag{3.39}$$

and substituted into Eq. 3.38 as

$$\boldsymbol{\phi M}^{-1}\left(\boldsymbol{p}+\boldsymbol{\phi}^{\boldsymbol{T}}\boldsymbol{\lambda}\right)=\boldsymbol{\gamma}. \tag{3.40}$$

After rearranging, the vector of the Lagrange's multipliers can be expressed as

$$\boldsymbol{\lambda}=\left(\boldsymbol{\phi M}^{-1}\boldsymbol{\phi}^{T}\right)^{-1}\left(\boldsymbol{\gamma}-\boldsymbol{\phi M}^{-1}\boldsymbol{p}\right). \tag{3.41}$$

When Eq. 3.41 is substituted into Eq. 3.37, vector $\boldsymbol{\lambda}$ can be eliminated from Eq. 3.37, thus vector of generalized accelerations can be expressed in form

$$\ddot{\boldsymbol{q}}=\mathbf{M}^{-1}\{\boldsymbol{p}+\boldsymbol{\phi}^{T}(\boldsymbol{\phi}\mathbf{M}^{-1}\boldsymbol{\phi}^{T})^{-1}(\boldsymbol{\gamma}-\boldsymbol{\phi}\mathbf{M}^{-1}\mathbf{p})\}. \tag{3.42}$$

Since the expression for accelerations without using vector multipliers have been obtained, the final system of matrix equation using the expressions and substitutions above can be written as

$$\begin{bmatrix}\dot{\boldsymbol{u}}\\ \boldsymbol{v}\end{bmatrix}=\begin{bmatrix}\boldsymbol{v}\\ \ddot{\boldsymbol{q}}\end{bmatrix}=\begin{bmatrix}\dot{\mathbf{q}}\\ \mathbf{M}^{-1}\{\boldsymbol{p}+\boldsymbol{\phi}^{T}(\boldsymbol{\phi}\mathbf{M}^{-1}\boldsymbol{\phi}^{T})^{-1}(\boldsymbol{\gamma}-\boldsymbol{\phi}\mathbf{M}^{-1}\mathbf{p})\}\end{bmatrix}. \tag{3.43}$$

This first order system of DAE can be solved using various numerical software. MATLAB [10] software is applied to figure out the proper numerical solution. Set of suitable numerical ODE solvers are implemented in MATLAB, such as ODE15s, ODE23, ODE45 and many others. Availability of specific solvers can be discussed. Generally, the stiffness or non-stiffness of particular differential equation is the main relevant factor for solver choice.

Eq. 3.43 can be solved using standard techniques of numerical integration, however it has some undesirable troubles. It is not numerically stable for a certain properties. Various methods describing and solving bad stability were developed [6]. One method is called the Baumgarte's stabilization.

The constrain equation $\ddot{\boldsymbol{\Phi}}=\mathbf{0}$ is modified as

$$\ddot{\boldsymbol{\Phi}}+2\alpha\dot{\boldsymbol{\Phi}}+\beta^{2}\boldsymbol{\Phi}=\mathbf{0} \tag{3.44}$$

and this is solved during numerical solution of Eq. 3.43. Constants α and β are chosen, recommended values can be found in [6].

Vector $\boldsymbol{\gamma}(\boldsymbol{q},\dot{\boldsymbol{q}},t)$ in Eq. 3.43 is replaced by the new one, namely

$$\bar{\boldsymbol{\gamma}}(\boldsymbol{q},\dot{\boldsymbol{q}},t)=\boldsymbol{\gamma}(\boldsymbol{q},\dot{\boldsymbol{q}},t)-2\alpha\dot{\boldsymbol{\Phi}}-\beta^{2}\boldsymbol{\Phi}. \tag{3.45}$$

This brings new formulation of the first order DAE, which is going to be numerically solved as

$$\begin{bmatrix}\dot{\boldsymbol{u}}\\ \dot{\boldsymbol{v}}\end{bmatrix} = \begin{bmatrix}\boldsymbol{v}\\ \ddot{\boldsymbol{q}}\end{bmatrix} = \begin{bmatrix}\dot{\mathbf{q}}\\ \mathbf{M}^{-1}\{\boldsymbol{p} + \boldsymbol{\Phi}^T(\boldsymbol{\Phi}\mathbf{M}^{-1}\boldsymbol{\phi}^T)^{-1}(\boldsymbol{\gamma}(\boldsymbol{q},\dot{\boldsymbol{q}},t) - 2\alpha\dot{\boldsymbol{\Phi}} - \beta^2\boldsymbol{\Phi} - \boldsymbol{\Phi}\mathbf{M}^{-1}\mathbf{p})\}\end{bmatrix}. \tag{3.46}$$

3.2 Contact calculation

The thesis concerns possible impacts between any ellipsoid of the double pendulum and a plain. If the pendulum bodies get into a collision, the crucial question is to evaluate impact performance of a contact force. Let us assume the recently used reference approaches for contact calculation, namely the discrete and continuous contact force models.

The continuous contact force model is chosen due to the simplicity of implementation for impact application where many bodies are tentatively in contact. So the force is a function of local indentation and indentation velocity respectively. Indentation or penetration between two bodies is here referred to δ. Fig. 3.4 depicts the interaction between two balls and quantity δ is displayed.

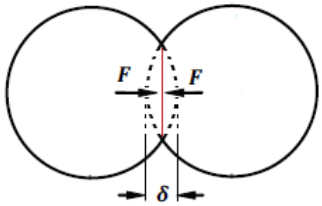

Figure 3.4: Two balls collision

To capture an effect of contact force in case of interaction of bodies, penetration depth has to be calculated. To identify whether the bodies are getting into a collision, the minimum distance between them is calculated. As long as the distance is positive, the bodies are disjointed. Change of the the sign indicates a collision and negative distance magnitude is equal to the penetration δ. Here, the double pendulum contact problem encroaches to two separated scenarios of particular body and a plain.

Several algorithms for minimum distance calculation were publicised [18, 21, 1, 4, 5, 2]. Recently most of public sources work with cycle computing the distance between set of points on the surfaces. Other approaches remain on collision detection algorithm [8, 14]. However, these are not evaluate indentation in case of overlapping bodies.

The literature review in Chapter 2 presents many methods for minimum distance calculation. An efficient method how to compute distance between ellipsoid and plain is the analytical one [19]. Due to the geometry simplicity of the double pendulum, this study is focused on analytical solution of minimum distance problem. Basic idea lies in creating a new plain, that is parallel to a given plain and touches the ellipsoid in just one point.

Since this point is detected, distance between the point and the plain can be calculated, using adequate equation of analytical geometry. As is shown in Fig. 3.5 there always exist two such parallel plains.

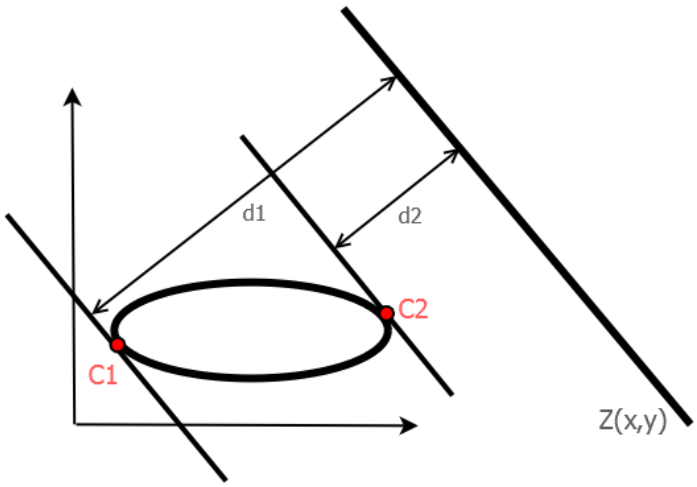

Figure 3.5: Parallel plains

3.2.1 Minimum distance problem application

Let us show the solution in the contact problem between an ellipsoid and a plain. General equation of an ellipsoid is given by a formula

$$\frac{x^2}{a^2} + \frac{y^2}{b^2} + \frac{z^2}{c^2} = 1, \tag{3.47}$$

where a, b and c are constants, which represent the length of semi-principal axes. Eq. 3.47 can be rearranged by set of substitution to the form

$$Ax^2 + By^2 + Cz^2 + D = 0, \tag{3.48}$$

where $A = \frac{1}{a^2}$, $B = \frac{1}{b^2}$, $C = \frac{1}{c^2}$ and $D = -1$. General equation of an arbitrary plain can be defined as

$$kx + ly + mz + n = 0. \tag{3.49}$$

Equation 3.49 can be rearrange to be a function $z = z(x, y)$ as

$$z(x, y) = -\frac{k}{m}x - \frac{k}{m}y - \frac{n}{m}. \tag{3.50}$$

Any arbitrary plain can be defined in several ways. One of suitable possibilities is to use one point and two vectors. To capture new plain being parallel with the initial one, at least two gradient vectors of both plains have to be the same. When two gradient vectors are developed, together with one point on ellipsoid, the required tangential plain is identified. Hence the gradients $\frac{\partial z}{\partial x}$ and $\frac{\partial z}{\partial y}$ of the plain $z = z(x, y)$ are being evaluated as

$$\frac{\partial z(x,y)}{\partial x} = -\frac{k}{m} \tag{3.51}$$

and

$$\frac{\partial z(x,y)}{\partial y} = -\frac{l}{m}. \tag{3.52}$$

To get a tangency parallel plain, the partial derivatives of Eq. 3.48 with respect to variables x and y are obtained as

$$\frac{\partial}{\partial x} : 2Ax + 2By \underbrace{\frac{\partial y}{\partial x}}_{0} + 2Cz \underbrace{\frac{\partial z}{\partial x}}_{-\frac{k}{m}} = 0 \tag{3.53}$$

and

$$\frac{\partial}{\partial y} : \; 2Ax \underbrace{\frac{\partial x}{\partial y}}_{0} + 2By + 2Cz \underbrace{\frac{\partial z}{\partial y}}_{-\frac{l}{m}} = 0. \tag{3.54}$$

Since x and y are independent variables, mutual derivations are equal to zero. When Eq. 3.51 and Eq. 3.52 are substituted into Eq. 3.53 and Eq. 3.54, together with general equation of ellipsoid Eq. 3.48, the system of three equations for unknown variables x, y and z is obtained as

$$2Ax - 2C\frac{k}{m}z = 0, \tag{3.55}$$

$$2By - 2C\frac{l}{m}z = 0 \tag{3.56}$$

and

$$Ax^2 + By^2 + Cz^2 + D = 0. \tag{3.57}$$

Solution of this system of equations provides two points $C_1 = [x_{10}, y_{10}, z_{10}]$ and $C_2 = [x_{20}, y_{20}, z_{20}]$, which are mutual points of the body and the tangential plain, also the

point of extrema distance (minimum and maximum) between the plain and the body, see Fig 3.5.

Since coordinates of these points are known, it is very straightforward to calculate distance between these points and the plain. The distance from point $\boldsymbol{X}_0 = [x_0, y_0, z_0]$ to plain $kx + ly + mz + n = 0$ is given by

$$d_i = \frac{kx_{i0} + ly_{i0} + mz_{i0} + n}{\sqrt{k^2 + l^2 + m^2}}, \text{where } i \in \{1, 2\}. \tag{3.58}$$

Eq. 3.58 gets two extrema distances between the ellipsoid and the plain, since minimum distance is required obviously as

$$d = min(d_1, d_2). \tag{3.59}$$

However, this elementary method is working only for ellipsoid, whose centre of gravity is located in the origin of the coordinate system and the semi-axes are identical with the coordinate axes. Here, in case of fixed plain and moving ellipsoid, Eq. 3.49 can be expressed on global, frame fixed coordinate system, but the equation of ellipsoid in desired form Eq 3.49 is evaluated on the local body fixed coordinate system.

Transformation

In this particular system, the plain is fixed, so it is time invariant and the location of ellipsoid is changing during the time. Actual position of any point on ellipsoid is defined with 6 independent coordinates $[x_s, y_s, z_s, \psi, \nu, \varphi]^T$ where x_s, y_s and z_s are COG coordinates and ψ, ν and φ are the Euler's angles.

plain and ellipsoid equations in elementary form 3.48 and 3.49 must be expressed in the same coordinate system, either local or global. As mentioned above, plain 3.49 is evaluate in global coordinate system and equation of ellipsoid Eq. 3.47 is in the local body fixed system. For the transformation, it is useful writing the plain and tha ellipsoid equations in a matrix form using homogeneous coordinates. Thus plain equation is

$$\begin{bmatrix} k & 0 & 0 & 0 \\ 0 & l & 0 & 0 \\ 0 & 0 & m & 0 \\ 0 & 0 & 0 & n \end{bmatrix} \cdot \begin{bmatrix} x \\ y \\ z \\ 1 \end{bmatrix} = \mathbf{0} \tag{3.60}$$

or in compact matrix form

$$\boldsymbol{RX} = \mathbf{0} \tag{3.61}$$

and the ellipsoid equation comes to

$$\begin{bmatrix} x & y & z & 1 \end{bmatrix} \begin{bmatrix} A & 0 & 0 & 0 \\ 0 & B & 0 & 0 \\ 0 & 0 & C & 0 \\ 0 & 0 & 0 & D \end{bmatrix} . \begin{bmatrix} x \\ y \\ z \\ 1 \end{bmatrix} = \mathbf{0} \tag{3.62}$$

or in matrix form

$$\boldsymbol{X}^T \boldsymbol{A} \boldsymbol{X} = \mathbf{0}. \tag{3.63}$$

The ellisposid takes spherical motion around COG described by tranformation matrix $\boldsymbol{T}_{12}$, see Eq. 3.6. Since centre of gravity is moving in time, transformation matrix $\boldsymbol{P}$ of translation (represented by x_s, y_s and z_s) is added. The matrix evaluated in homogeneous coordinates

$$P = \begin{bmatrix} 1 & 0 & 0 & x_s \\ 0 & 1 & 0 & y_s \\ 0 & 0 & 1 & z_s \\ 0 & 0 & 0 & 1 \end{bmatrix} \tag{3.64}$$

where $x_s(t)$, $y_s(t)$ and $z_s(t)$ are coordinates of body COG that are functions of time.

Final matrix to transforming any point from local system 2 to global 1 is derived using the rule for compound transformation

$$\boldsymbol{T} = \boldsymbol{P}\boldsymbol{T}_{12}. \tag{3.65}$$

Note, that transformation matrix from system 1 to 2 is

$$\tilde{\boldsymbol{T}} = \boldsymbol{T}^{-1} = \boldsymbol{T}_{12}^{-1}\boldsymbol{P}^{-1} = \boldsymbol{T}_{21}\boldsymbol{P}^{-1}. \tag{3.66}$$

The very crucial phenomenon is how to transform those equations to be expressed in the same coordinate system and obtain equations in such a form, which the methods of distance calculation can be applied on.

There are two possibilities to assure both of the bodies in the same coordinate system:

- The first one is using matrix $\boldsymbol{T}$ to transform ellipsoid Eq 3.63 from the local coordinate to the global one (where the plain is defined) as

$$\boldsymbol{X}^T\boldsymbol{T}^T\boldsymbol{A}\boldsymbol{T}\boldsymbol{X} = \mathbf{0}. \tag{3.67}$$

- The second one is to use matrix $\tilde{\boldsymbol{T}}$ to transform plain Eq. 3.61 from the global coordinate system to the local one (where the ellipsoid is defined) as

$$\boldsymbol{R\tilde{T}X} = \mathbf{0}. \tag{3.68}$$

The first option gives a scalar equation, but it is highly non-linear and it is not possible to arrange that in a form $\tilde{A}x^2 + \tilde{B}y^2 + \tilde{C}z^2 + \tilde{D} = 0$, where $\tilde{A}$, $\tilde{B}$, $\tilde{C}$ and $\tilde{D}$ can be any arbitrary matrices. So, this option is not possible for this purpose.

The second option provides vector equation of dimension 4. In order to evaluate the scalar plain equation in the new coordinate (local body-fixed) system, all the rows of Eq. 3.68 need to be summarised. Obtained scalar equation of the plain can be written in the same form as the original one as

$$\tilde{k}x + \tilde{l}y + \tilde{m}z + \tilde{n} = 0 \tag{3.69}$$

where $\tilde{k}$, $\tilde{l}$, $\tilde{m}$, $\tilde{n}$ are constants defined by particular transformation,

$$\tilde{k} = k\,c(\varphi_\mathrm{i})\;c(\psi_\mathrm{i}) - l\,c(\psi_\mathrm{i})\;s(\varphi_\mathrm{i}) + m\,s(\nu_\mathrm{i})\;s(\psi_\mathrm{i}) - l\,c(\varphi_\mathrm{i})\;c(\nu_\mathrm{i})\;s(\psi_\mathrm{i}) - k\,c(\nu_\mathrm{i})\;s(\varphi_\mathrm{i})\;s(\psi_\mathrm{i})\,, \tag{3.70}$$

$$\tilde{l} = k\,c(\varphi_\mathrm{i})\;s(\psi_\mathrm{i}) - m\,c(\psi_\mathrm{i})\;s(\nu_\mathrm{i}) - l\,s(\varphi_\mathrm{i})\;s(\psi_\mathrm{i}) + l\,c(\varphi_\mathrm{i})\;c(\nu_\mathrm{i})\;c(\psi_\mathrm{i}) + k\,c(\nu_\mathrm{i})\;c(\psi_\mathrm{i})\;s(\varphi_\mathrm{i})\,, \tag{3.71}$$

$$\tilde{m} = k\,c(\varphi_\mathrm{i})\;c(\psi_\mathrm{i}) - l\,c(\psi_\mathrm{i})\;s(\varphi_\mathrm{i}) + m\,s(\nu_\mathrm{i})\;s(\psi_\mathrm{i}) - l\,c(\varphi_\mathrm{i})\;c(\nu_\mathrm{i})\;s(\psi_\mathrm{i}) - k\,c(\nu_\mathrm{i})\;s(\varphi_\mathrm{i})\;s(\psi_\mathrm{i}) \tag{3.72}$$

and

$$\tilde{n} = d + k\,\mathrm{x_{si}} + l\,\mathrm{y_{si}} + m\,\mathrm{z_{si}} \tag{3.73}$$

where c is for cosine and s is for sine.

Now both (plain and ellipsoid) equations are in one coordinate system (local body-fixed) and the standard distance calculation method described above can be used. There is only one difference in using general transformed parameters $\tilde{k}$, $\tilde{l}$, $\tilde{m}$ and $\tilde{n}$ instead of k, resp. l, m and n.

It does not make any problem that the distance is calculated in local coordinate system. The applied transformations are only translations and rotations, which are kind of affine transformations. Using affine transformation, the distance between two point is not changing, so it is invariant to that particular transformation.

However, any vector is not invariant to that. When any vector is obtained in the local coordinate system, for example location vector of the contact point, the external normal

vector or the contact force vector has to be transformed using matrix $\boldsymbol{T}_{12}$ to get that in the desired form.

Equation of a transformed plain Eq. 3.69 together with original equation of ellipsoid 3.48 are satisfactory input to calculate the minimum distance. Solving system of equations, two points of extrema distance C_1 and C_2 are evaluated. Next step is just using expression Eq. 3.58 for distance calculation with the transformed coefficients,

$$d_i = \frac{\tilde{k}x_{i0} + \tilde{l}y_{i0} + \tilde{m}z_{i0} + \tilde{n}}{\sqrt{\tilde{k}^2 + \tilde{l}^2 + \tilde{m}^2}}, \quad i \in \{1, 2\}. \tag{3.74}$$

Required distance between the body and the plain is obviously

$$d = min(d_1, d_2). \tag{3.75}$$

3.2.2 Contact force

Several normal contact force models are at present used to identify encroaching force due to impact. This study is focused on continuous models implementation, in which impacting force is defined to be a function of penetration. Relative normal contact velocity is thus

$$\vec{\boldsymbol{F}}_{\boldsymbol{n}} = \vec{\boldsymbol{F}}_{\boldsymbol{n}}(\delta, \dot{\delta}). \tag{3.76}$$

Minimum distance problem was described above, as mentioned, negative magnitude of distance indicated overlapping of bodies. Assuming references of some commercial software, contact thickness parameter is introduced. When δ become less then constant h_{cont} normal force is being calculated and implemented to the system. Normal contact force acts in negative direction of external normal vector of ellipsoid, see Fig 3.6.

General form of the external normal vector of an ellipsoid $Ax^2 + By^2 + Cz^2 + D = 0$ is

$$\vec{\boldsymbol{n}} = [A, B, C]^T. \tag{3.77}$$

External normal vector located at the contact point in local body coordinate system is defined with

$$\vec{\boldsymbol{n}}_{loc}^{cE} = \vec{\boldsymbol{n}}\ \vec{\boldsymbol{r}}_{loc}^{c}, \tag{3.78}$$

where $\vec{\boldsymbol{n}}$ is external normal vector defined above, $\vec{\boldsymbol{r}}_{loc}^{c}$ are coordinates of contact point in local coordinate system.

Since unitary vector of internal normal is required, vector $\vec{\boldsymbol{n}}_{loc}^{cE}$ is normalized and multiplied with (-1) to generated desired vector

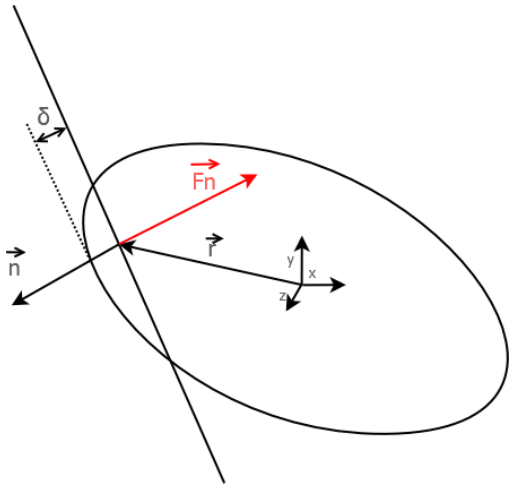

Figure 3.6: Acting normal contact force

$$\vec{\boldsymbol{n}}^{c}_{loc} \equiv \vec{\boldsymbol{n}}^{cI}_{loc} = (-1)\ \frac{\vec{\boldsymbol{n}}^{cE}_{loc}}{\parallel \vec{\boldsymbol{n}}^{cE}_{loc} \parallel}. \tag{3.79}$$

Normal vector expressed in global coordinates is developed applying transformation between local and global coordinate system,

$$\vec{\boldsymbol{n}}^{c}_{gl} = \boldsymbol{T}_{12}\ \vec{\boldsymbol{n}}^{c}_{loc}. \tag{3.80}$$

Coordinates vector of contact point in global coord. system is evaluated using general transformation relationship (translation and spherical rotation)

$$\vec{\boldsymbol{r}}^{c}_{gl} = \vec{\boldsymbol{X}}_{\boldsymbol{s}} + \boldsymbol{T_{12}}\ \vec{\boldsymbol{r}}^{c}_{loc}. \tag{3.81}$$

Calculation of relative normal contact velocity (indentation velocity) is not so straightforward. Some guidelines define this to be only a velocity of contact point in direction of external normal. However, it does not sound physically relevant. To capture a pure effect of penetration velocity Eq 3.58 is derivatived. Since computing of penetration is evaluated in body fixed local coordinate system, coordinates of contact point are constants and position of plain is changing with time. Thus $x_0,\ y_0, z_0$ are constants and quantities k, l, m, n are functions of time. Penetration velocity is so developed using this equation,

$$\frac{d}{dt}\delta = \dot{\delta} = \frac{d}{dt}\left\{\frac{kx_0 + ly_0 + mz_0 + n}{\sqrt{k^2 + l^2 + m^2}}\right\} \equiv \frac{\dot{f}g - f\dot{g}}{g^2}, \tag{3.82}$$

where

$$f = kx_0 + ly_0 + mz_0 + n, \tag{3.83}$$

$$g = \sqrt{k^2 + l^2 + m^2}, \tag{3.84}$$

$$\dot{f} = \frac{df}{dt} = \dot{k}x_0 + \dot{l}y_0 + \dot{m}z_0 + \dot{n}, \tag{3.85}$$

$$\dot{g} = \frac{dg}{dt} = \frac{1}{2}(k^2 + l^2 + m^2)^{-\frac{1}{2}}(2k\dot{k} + 2l\dot{l} + 2m\dot{m}), \tag{3.86}$$

and quantities $\dot{k},\ \dot{l},\ \dot{m},$ are derivatives of Eqs. 3.70, 3.71 and 3.72, respectively.

Vector of contact force $\vec{\boldsymbol{F}}^c_{gl}$ can be evaluated using entities above, regarding adequate contact force model:

- Hertz
$$\vec{\boldsymbol{F}}^c_{gl} = \boldsymbol{F_n}\vec{\boldsymbol{n}}^c_{gl} = k_h\ \delta^n\ \vec{\boldsymbol{n}}^c_{gl} \tag{3.87}$$
- Spring dashpot
$$\vec{\boldsymbol{F}}^c_{gl} = \boldsymbol{F_n}\vec{\boldsymbol{n}}^c_{gl} = (k_{sd}\ \delta\ + b_{sd}\ \dot{\delta})\vec{\boldsymbol{n}}^c_{gl} \tag{3.88}$$
- Non-linear
$$\vec{\boldsymbol{F}}^c_{gl} = \boldsymbol{F_n}\vec{\boldsymbol{n}}^c_{gl} = (k_{nl}\ \delta^n\ + b_{nl}\ \delta^n\dot{\delta})\vec{\boldsymbol{n}}^c_{gl} \tag{3.89}$$

Acting force $\vec{\boldsymbol{F}}^c_{gl}$ is then translated to the centre of gravity of the body and including a moment $\vec{\boldsymbol{M}}^c_{gl}$ cause by translation. Figure 3.7 shows two equivalent systems, first one with contact force acting at contact point, and second system loaded with force acting in COG and a moment.

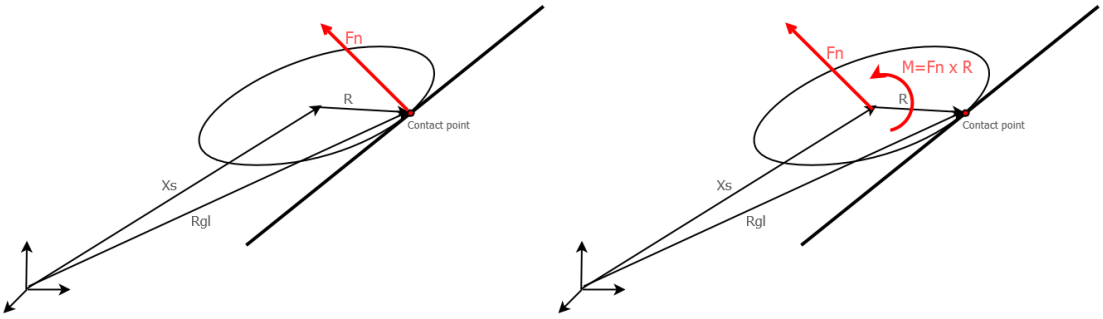

(a) Original position of contact force (b) Translated force and a moment

Figure 3.7: Two equivalent systems

Moment is obviously calculated from

$$\vec{\boldsymbol{M}}^c_{gl} = \vec{\boldsymbol{R}} \times \vec{\boldsymbol{F}}^c_{gl}, \tag{3.90}$$

where vector $\vec{\boldsymbol{R}}$ can be expressed using position vector of contact point $\vec{\boldsymbol{r}}^{c}_{gl}$ and COG coordinates $\vec{\boldsymbol{X}}_{\boldsymbol{s}}$, regarding Fig 3.7

$$\vec{\boldsymbol{R}} = \vec{\boldsymbol{r}^{c}_{gl}} - \vec{\boldsymbol{X}}_{\boldsymbol{s}}. \tag{3.91}$$

Force implementation

In case of contacting bodies right hand side of equation of motion Eq. 3.46 comes to following form

$$\boldsymbol{f} = \begin{bmatrix} \boldsymbol{F}^{c}_{gl}\ \boldsymbol{e_1} \\ \boldsymbol{F}^{c}_{gl}\boldsymbol{e_2} \\ -mg + \boldsymbol{F}^{c}_{gl}\boldsymbol{e_3} \\ \boldsymbol{M}^{cx}_{gl} \\ \boldsymbol{M}^{cy}_{gl} \\ \boldsymbol{M}^{cz}_{gl} \end{bmatrix} = \begin{bmatrix} \boldsymbol{F}^{cx}_{gl} \\ \boldsymbol{F}^{cy}_{gl} \\ -mg + \boldsymbol{F}^{cz}_{gl} \\ \boldsymbol{M}^{cx}_{gl} \\ \boldsymbol{M}^{cy}_{gl} \\ \boldsymbol{M}^{cz}_{gl} \end{bmatrix} \tag{3.92}$$

For a case of disjoint bodies, $\boldsymbol{F}_n = 0$ and thus vector $\vec{\boldsymbol{f}}$ comes to simply form of unconstrained model loaded only with a gravity.

$$\boldsymbol{f} = \begin{bmatrix} 0 \\ 0 \\ -mg \\ 0 \\ 0 \\ 0 \end{bmatrix}. \tag{3.93}$$

To sum up effect of penetration and contact force, respective, adding to equation of motion, a flowchart is given.

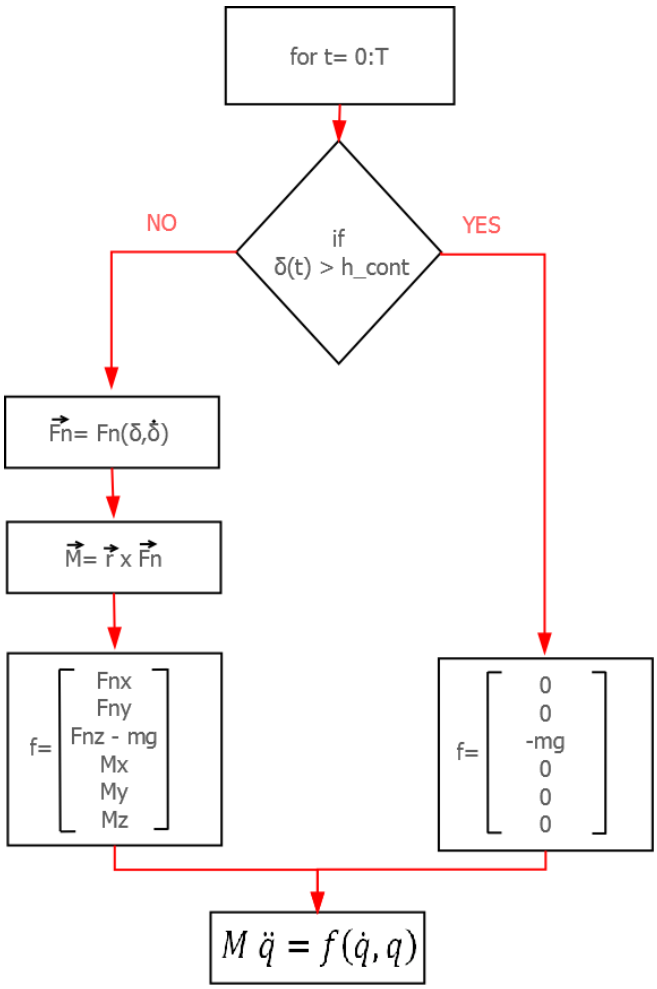

Figure 3.8: Flowchart of ODE solution

3.3 Contact parameters optimization

In previous part the main three continuous normal contact force models were presented. Namely Herz's model, spring-dashpot and non-linear damping model. All the three principles define normal force to be function of relative normal deformation between the contacting bodies δ and indentation velocity $\dot{\delta}$, respectively, and set of theoretical parameters.

Normal force model definitions:

- Hertz's model

$$F_n = k_h \delta^n \tag{3.94}$$

- Spring-dashpot model

$$F_n = k_{sd}\delta + b_{sd}\dot{\delta} \tag{3.95}$$

- Non-linear damping model

$$F_n = k_{nl}\delta^n + b_{nl}\delta^p\dot{\delta}^q \tag{3.96}$$

However, all the parameters are only theoretical values approximating effect of real force generated during impact. Definitions formulas, how to calculate particular parameters, were derived, but only for special case [9]. Recently, the common published one deals with contact of two spheres in 2D space. Quantity k_i representing stiffness parameter and b_i representing damping coefficient, respectively are functions of material and geometric properties of contacting bodies. In case of 2D spheres impact, k is defined by formula

$$k = \frac{4}{3(\sigma_i + \sigma_j)} \left[\frac{R_i R_j}{R_i + R_j}\right]^{\frac{1}{2}}, \tag{3.97}$$

in which the parameters σ_i and σ_j are given by formula

$$\sigma_s = \frac{1 - \nu_s^2}{E_s}, \text{ where s=\{i,j\}} \tag{3.98}$$

Where quantities E_s and ν_s are Young's modulus and a Poisson's ratios associated with material of each spheres, respectively.

In general case, for example 3D, eccentric contact etc., it is not possible to derive desired expressions. Since all force models should approximate a real case, experimental results are used and compared with simulations to carry out appropriate values of parameters k_i and b_i, respectively. By varying the theoretical quantities, the most corresponding results

of simulation to an original experiment can be achieved. This mathematical method is called optimization, for example gradient based optimization. Main principle is shown in the flowchart

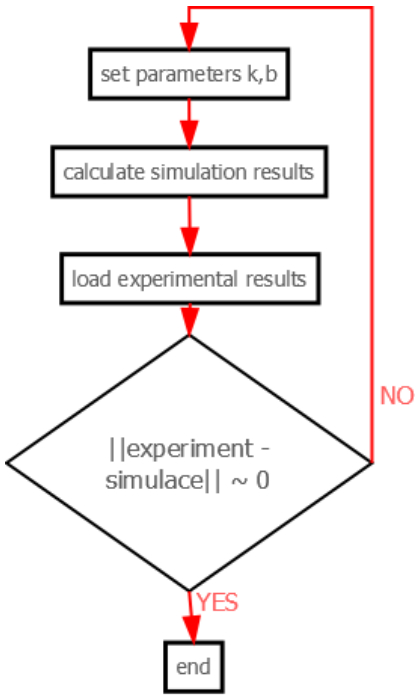

Figure 3.9: Flowchart of optimization

Numerical optimization is highly complicated mathematical process and it is not the purpose of this work to described that, so it is not being discussed.

This particular scenario is a problem of multi-parameters optimization, together with one objective function. Namely stiffness and damping parameters are active values and difference between experimental and calculated results is an objective function, which is desirable to be minimised.

Public sources provide not very wide set of a suitable experiments. However, [9] publicised elementary application suitable for validation. The example of application considered here is bouncing ball in 2D, which is one of the simplest mechanical contact system. However, this is not an experimental result. The article [9] contains only an application simulation example results. Nevertheless, simulation that had been already verified, can also render appropriate data to validate a new model.

Figure 3.10 shows an elastic ball with an initial height equals to 1.0 m, mass of 1 kg, moment of inertia equals to 0.1 $kg.m^2$ and radius equals to 0.1 m. The ball is releases from initial position under action only of gravity g equals to 9.81 $m.s^{-2}$. Ball is falling down until it collides with a rigid and stationary ground. When the ball collides a contact takes place and ball rebounds, producing jump, which height is depending on parameters

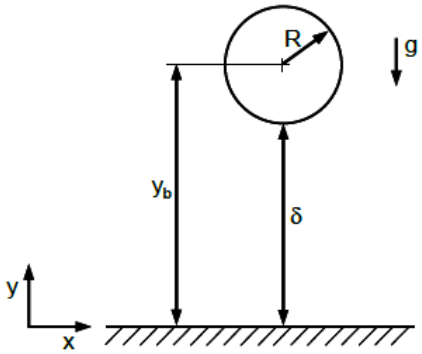

Figure 3.10: Bouncing ball example [9]

of the normal force. The quantity which is shown is position of centre of gravity of the ball in the time, thus namely the y coordinate.

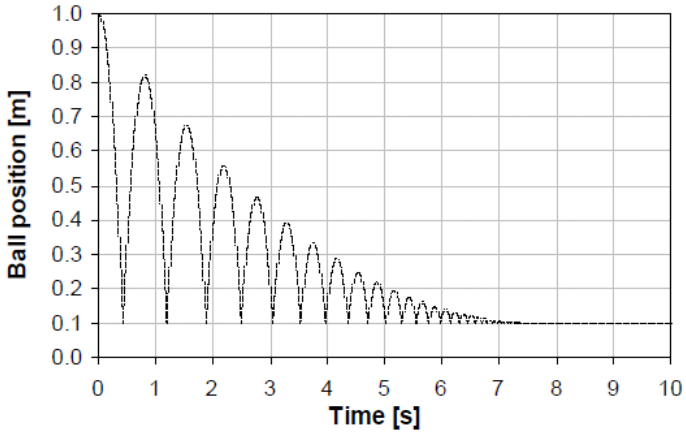

Figure 3.11: Ball position [9]

Software optiSlang, version optiSlang 3.2.0 is a suitable program to apply required optimization principle. It is developed to cooperate with numerous of software to reach results that capture minimization of an objective function. In this case MATLAB software calculates motion of a ball and optiSlang is controlling a variation of input parameters k and b, respectively. An output from MATLAB is a difference between simulation and experiment. This function comes to be objective function for optiSlang.

$$Obj = (simulation - experiment)^2. \tag{3.99}$$

Cause the experimental results are set of discrete values, points difference was calculated

$$Obj(i) = (simulation(i) - experiment(i))^2 \text{i} \in \{1, 2, ..., T_{max}\} \tag{3.100}$$

Since optiSlang can not work with objective function to be a proper function, it is working only with single value. Sum of differences needs to be done.

$$Obj \equiv Obj(i) = \sum_{i=0}^{N} (simulation(i) - experiment(i))^2. \tag{3.101}$$

where N represents number of experimental curve points. Square root is used to avoid zeroing of values with opposite sign. This could be ensure only by using absolute value, but it can cause non-smoothness in solution. Hence an output from MATLAB programme is one single value representing difference between curves of experiment and simulation. This number is then input for optiSlang,in which is desirable to be minimised.

All the normal contact models Eq. 3.94, 3.95, 3.96 were put-upon optimization process to reach appropriate values of stiffness and damping quantities.

3.3.1 Bouncing ball theory

Bouncing ball is classical elementary contact system. It contains one free body (ball) and a rigid frame (ground). Purpose of this study is to built a suitable model, which can be compared with appropriate results, to validate particular contact models. In previous section EOM of double pendulum was derived using Lagrange's equation principle. Later on, some external forces, caused by local indentation were added to the system. Free bouncing sphere (ball) with radius equals to r is only a special case of pendulum movement, namely pendulum with semi-axis $a_i = r$, for $i \in \{1, 2, 3\}$. When this body is not subjected to any constraints, it comes to be a free body movement.

Due to this assumption, double pendulum EOM can be modified to capture free bouncing ball EOM. However, this can makes a model slightly unclear. In order to avoid this uncertainties, new EOM is derived using the same principle used previous.

Equation of motion of free ball

Principle of developing equation of motion of free body movement is similar with double pendulum motion. However, there are no constraints in the system. Lagrange's equation of a first kind is applied to obtain EOM.

General formula of Lagrange's equation is

$$\frac{d}{dt}\frac{\partial E_k}{\partial \dot{q}_i} - \frac{\partial E_p}{\partial q_i} = \mathbf{0}, \text{ i} \in \{1.....6\} \tag{3.102}$$

Kinetic energy of the system is then

$$E_k = \frac{1}{2}\sum \dot{\boldsymbol{q}}^T \boldsymbol{M} \dot{\boldsymbol{q}} \tag{3.103}$$

,
where $\boldsymbol{q}$ is vector of generalized coordinates, namely:

$$\mathbf{q} = [x_s, y_s, z_s, \psi, \nu, \varphi]^T.$$

Potential energy of the system is

$$E_p = -mgq_3 = -mgz_s. \tag{3.104}$$

Derivatives of kinetic energy with respect to general velocities (derivatives of coordinates) comes to a form, that is recently derivatives with respect to time

$$\frac{d}{dt}\frac{\partial E_k}{\partial \dot{q}_i} = \boldsymbol{M}\ddot{\boldsymbol{q}}, \tag{3.105}$$

where $\boldsymbol{M}$ is a mass matrix.

Derivatives of potential energy with respect to general coordinates

$$\frac{\partial E_p}{\partial q_i} = 0, \text{ for i} \in \{1, 2, 4, 5, 6\}, \tag{3.106}$$

and

$$\frac{\partial E_p}{\partial q_i} = -mg, \text{ for i} = 3. \tag{3.107}$$

Thus, the equation of motion comes to a form

$$\boldsymbol{M}\ddot{\boldsymbol{q}} = \boldsymbol{f}, \tag{3.108}$$

where $\ddot{\boldsymbol{q}}$ denotes a general acceleration vector and $\boldsymbol{f}$ is a vector generalized force.

Equation 3.108 can be written components form

$$\begin{bmatrix} \mathrm{m} & 0 & 0 & 0 & 0 & 0 \\ 0 & \mathrm{m} & 0 & 0 & 0 & 0 \\ 0 & 0 & \mathrm{m} & 0 & 0 & 0 \\ 0 & 0 & 0 & \mathrm{I}_1 & 0 & 0 \\ 0 & 0 & 0 & 0 & \mathrm{I}_2 & 0 \\ 0 & 0 & 0 & 0 & 0 & \mathrm{I}_3 \end{bmatrix} \begin{bmatrix} \ddot{q}_1 \\ \ddot{q}_2 \\ \ddot{q}_3 \\ \ddot{q}_4 \\ \ddot{q}_5 \\ \ddot{q}_6 \end{bmatrix} = \begin{bmatrix} F_x \\ F_y \\ F_z \\ M_x \\ M_y \\ M_z \end{bmatrix}, \tag{3.109}$$

or

$$\begin{bmatrix} \mathrm{m} & 0 & 0 & 0 & 0 & 0 \\ 0 & \mathrm{m} & 0 & 0 & 0 & 0 \\ 0 & 0 & \mathrm{m} & 0 & 0 & 0 \\ 0 & 0 & 0 & \mathrm{I}_1 & 0 & 0 \\ 0 & 0 & 0 & 0 & \mathrm{I}_2 & 0 \\ 0 & 0 & 0 & 0 & 0 & \mathrm{I}_3 \end{bmatrix} \begin{bmatrix} \ddot{x}_s \\ \ddot{y}_s \\ \ddot{z}_s \\ \ddot{\psi} \\ \ddot{\nu} \\ \ddot{\varphi} \end{bmatrix} = \begin{bmatrix} 0 \\ 0 \\ -mg \\ 0 \\ 0 \\ 0 \end{bmatrix} \tag{3.110}$$

Equation 3.110 describes free, unconstrained body system. To demonstrate bouncing ball with a contact implementation, external normal force need to be add in right hand side (later referred as RHS) of the model, as was discussed above. All the three main force interpretations are introduced.

Phenomena of contact force calculation is based on computing penetration (δ) between body and plain. In every time step, minimum distance between body is being computed. In case of $\delta < h_{cont}$, which indicates a collision, normal force is calculated and added to system, assuming particular model.

3.3.2 *IF* problem

In this section problem of discontinuities caused by *IF* condition presented in Fig 3.8 is described and solved. Precept of *IF* condition seems to be very simple, with no trouble. However, this brings irregularities in numerical integration.

If there is no penetration ($\delta > 0$, $\delta > h_{cont}$, respectively), system Eq 3.118 is subjected only to a gravitation, thus vector of external forces is

$$\boldsymbol{f} = \begin{bmatrix} 0 \\ 0 \\ -mg \\ 0 \\ 0 \\ 0 \end{bmatrix}. \tag{3.111}$$

If $\delta < h_{cont}$ that indicates the impact of body and ground, normal contact force is calculated and added to the RHS of system. Let assumed first contact occur in time $t = T_c$. It signifies some value (non-zero)of contact force at this time, but force equals to zero at $t < T_c$. Thus the force diagram is discontinuous and non-smooth, see fig 3.12.

Whatever small value of time step is set, it always generates a step change of force, from zero to a non-zero value. Due to this fact, it causes discontinuities in ODE solution, respectively in process of numerical integration. Functions ODE implemented in MATLAB software are used to evaluate a solution. When the *IF* approach is used, the solution is usually found. The crucial question is calculation time and a stability of numerical integration. To avoid this effect, *if* condition is replaced by special form of a Heaviside step

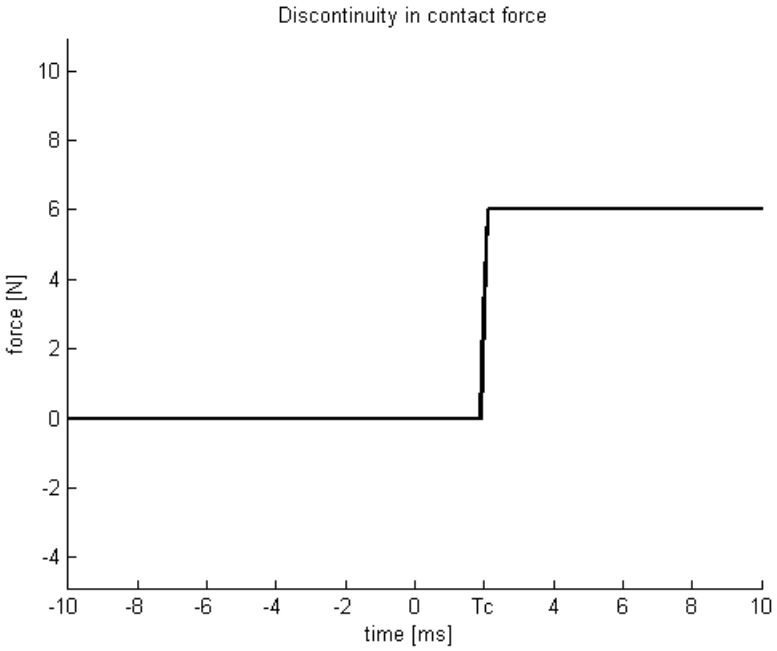

Figure 3.12: Contact force discontinues

function. Classical Heaviside function, usually marked as H, is discontinuous function that value is zero for negative argument and equals to one for positive argument. For a smooth approximation of H function, some analytical functions are known [22].

In this particular example a classical approximation needs to be modified to catch the proper *IF* condition problem.

- If condition:

$$IF: \ \delta < h_{cont}$$

  where δ represents distance between bodies.

- Modified $H(\delta)$ function:

$$H(\delta) = \lim_{k\to\infty} \frac{1}{2} + \frac{1}{\pi} \arctan(-k(\delta - h_{con})) \tag{3.112}$$

Application of Heaviside step function into a contact force model, the necessity of using *IF* condition is reduced. Contact force is then calculated in every time step following particular force definition including Heaviside function.

- Hertz's model

$$F_n = k_h \delta^n H(\delta) \tag{3.113}$$

- Spring-dashpot model

$$F_n = \left[k_{sd}\delta + b_{sd}\dot{\delta}\right]\ H(\delta) \tag{3.114}$$

- Non-linear damping model

$$F_n = \left[k_{nl}\delta^n + b_{nl}\delta^p\dot{\delta}^q\right]\ H(\delta) \tag{3.115}$$

3.3.3 Numerical optimization

Free ball motion acting a contact with rigid ground system has then equation of motion in form

$$\begin{bmatrix} \mathrm{m} & 0 & 0 & 0 & 0 & 0 \\ 0 & \mathrm{m} & 0 & 0 & 0 & 0 \\ 0 & 0 & \mathrm{m} & 0 & 0 & 0 \\ 0 & 0 & 0 & \mathrm{I}_1 & 0 & 0 \\ 0 & 0 & 0 & 0 & \mathrm{I}_2 & 0 \\ 0 & 0 & 0 & 0 & 0 & \mathrm{I}_3 \end{bmatrix} \begin{bmatrix} \ddot{x}_s \\ \ddot{y}_s \\ \ddot{z}_s \\ \ddot{\psi} \\ \ddot{\nu} \\ \ddot{\varphi} \end{bmatrix} = \begin{bmatrix} \boldsymbol{F_n e_1} \\ \boldsymbol{F_n e_2} \\ \boldsymbol{F_n e_3} - mg \\ \boldsymbol{M_{23}} \\ \boldsymbol{M_{13}} \\ \boldsymbol{M_{12}} \end{bmatrix}. \tag{3.116}$$

In which $\boldsymbol{F_n}$ is acting force regarding particular contact model and $\vec{\boldsymbol{M}}_{ij}$, i, j $\in \{1, 2, 3\}$ is generated moment equals to $\vec{\boldsymbol{M}} = \vec{\boldsymbol{R}} \times \vec{\boldsymbol{F_n}}$ and $\vec{\boldsymbol{e_i}}$ represent bases of the space.

Eq. 3.116 is write in matrix form

$$\mathbf{M}\ \ddot{\boldsymbol{q}} = \boldsymbol{f} \tag{3.117}$$

Equations 3.116 and 3.117, represent system of second-order differential equation (ODE). Principle of solution such equations was described. It can be transformed to a system, which is possible to solved in a numerical way

$$\begin{bmatrix} \dot{\boldsymbol{u}} \\ \boldsymbol{v} \end{bmatrix} = \begin{bmatrix} \boldsymbol{v} \\ \ddot{\boldsymbol{q}} \end{bmatrix} = \begin{bmatrix} \dot{\boldsymbol{q}} \\ \boldsymbol{M}^{-1}\boldsymbol{f} \end{bmatrix}. \tag{3.118}$$

MATLAB software version R2011b under Ms Windows platform on single processor Core Duo T2400 computer with frequency of 1.83 GHz a 2 MB L2 cache, is being used to numerically solve example of free ball motion. Based on a theory [6], Eq. 3.118 symbolize so called stiff differential equation problem. MATLAB has implemented several numerical

solver suitable for the stiff problems. However, it is not very straightforward to select a best one. In order to evaluate stable results and minimize calculation time, four stiff numerical solver ODE are applied on the same system. Simulation of bouncing ball example at 1 sec. and 5 sec. duration time are worked out, respectively.

	Computation time [s]	
Solver	1 sec. simulation	5 sec. simulation
ODE23t	169	1820
ODE23tb	278	2675
ODE15s	166	1382
ODE23s	1592	20 045

Table 3.1: Calculation time of identical simulation with different solvers

Table 3.1 results in acknowledgement of the type of solvers which are the most suitable . Four solvers were applied onto identical system and as can be seen computational time differs. One can observe, that ODE23s is definitely not suitable solver for this particular stiff differential equation. On the other hand, ODE23t and ODE15s appear to be a good choice. In this computation ODE15s solver was implemented for numerical solution.

Chapter 4

Results and discussion

Aim of this part is to present and discuss achieved results. At the beginning, motion of double pendulum system is going to be validated. For this purpose, experiment and published simulation of an arm motion is used and compared with calculated results. In the next, bouncing ball example is presented. This application contains numerical optimization principle in order to identify particular values of contact parameters for all three models. Thus results of bouncing ball motion using Hertz, spring-dashpot and nonlinear damping model are displayed. The contact force generated during the impact of this example is shown and compared with results of initial experiment. Suitable applications of this model in biomechanics are reported. At the first, example of the double pendulum contacting a plain, which can represent impact of arm with a structure. Second biomechanics application is a leg form example getting into collision with plain.

4.1 Free double pendulum motion

In part 3.1 equation of motion of double pendulum with no collision was evaluated. The following set of figures displays sequence of double pendulum motion. First body has mass $m_1 = 1kg$, moments of inertia $I_{11} = 2, I_{12} = 3, I_{13} = 1$ and semiaxes $a_{11} = a_{12} = 1$ and $a_{13} = 2$. Second body of double pendulum has mass $m_2 = 1kg$, moments of inertia $I_{21} = 2, I_{22} = 3, I_{23} = 1$ and semiaxes $a_{21} = a_{22} = 1$ and $a_{23} = 2$. The simulation starts with horizontal position of both bodies with initial velocities equal to zero. Thus only gravitation is loading the system. Position in time $t \in \{0, 0.5, 1, 1.5, 2, 2.5\}$ is displayed.

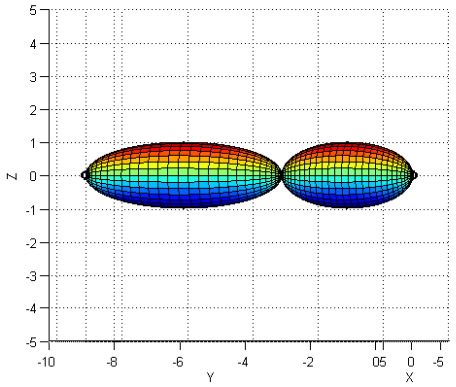

Figure 4.1: Position of double pendulum at t=0 sec

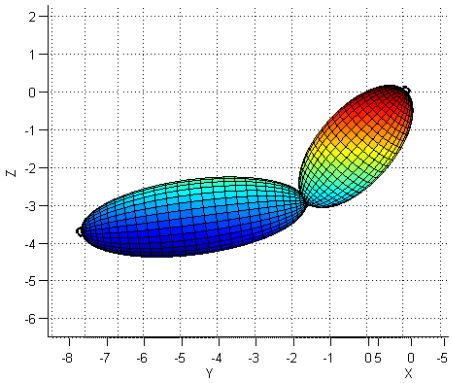

Figure 4.2: Position of double pendulum at t=0.5 sec

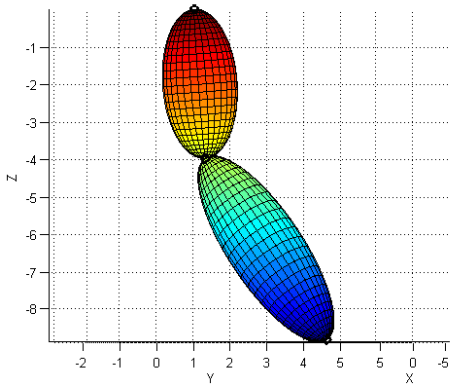

Figure 4.3: Position of double pendulum at t=1sec

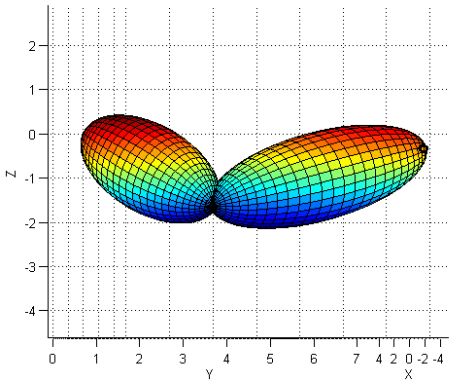

Figure 4.4: Position of double pendulum at t=1.5 sec

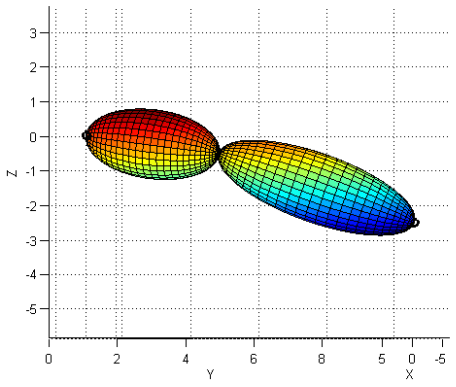

Figure 4.5: Position of double pendulum at t=2 sec

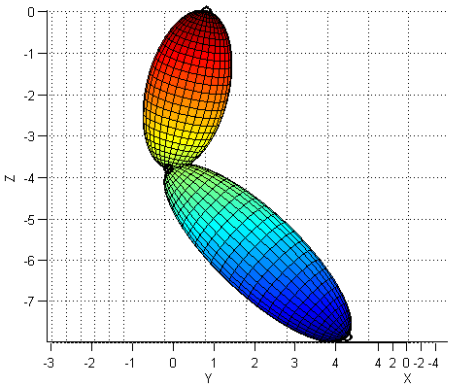

Figure 4.6: Position of double pendulum at t=2.5 sec

4.2 Arm gravity motion

Double pendulum system can be used in biomechanical fields to approximate various segments of a human body, such as arm and leg. Valdmanová in [20] established a 2D model of an arm based on multibody approach. This model consists of three elliptical bodies constrained together. These bodies represent the main part of a human arm, namely the upper arm, the forearm and the hand. Later on, model was simplified into a two bodies system only, since the motion between forearm and hand can be neglected. Geometric properties of two bodies model were transformed to catch the behaviour of the system influenced by a hand. Valdmanová assumed all the bodies with uneven mass distribution, thus the COG does not lay on the centre of ellipse. This effect is not considered in this work. Valdmanová compared in her work simulation with result of an experiment. Joints between bodies are modelled to be joints with an internal stiffness. Thus the bodies load with moments representing thickness of a shoulder and of an elbow, respectively. Geometric properties of the bodies are set of from [20] and are displayed in table 4.1.

Parameter	Units	Upper Arm	Forearm
Moments of inertia $I_\psi = I_\nu = I_\varphi$	$[Kg.m^2]$	0.0126	0.0105
Length of semi-axes $a_1 = a_2$	$[m]$	0.044	0.0314
Length of semi-axis a_3	$[m]$	0.1574	0.3345
Mass m	$[Kg]$	1.9807	2.5853

Table 4.1: Geometric parameters of the bodies

Passive bending moments of joints are defined by curves based on Robbinse [17], see figures 4.7, 4.8.

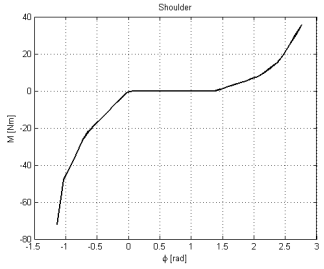

Figure 4.7: Passive bending moment of a shoulder

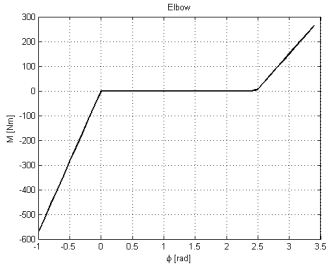

Figure 4.8: Passive bending moment of an elbow

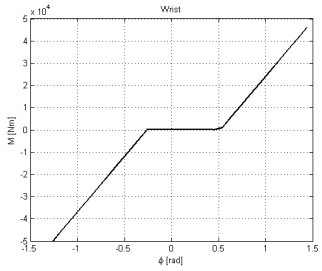

Figure 4.9: Passive bending moment of a wrist

Due to the effect of passive moments, exerting on the bodies, right hand side of equation of motion comes to a formula

$$\boldsymbol{f} = \begin{bmatrix} 0 \\ 0 \\ -m_1 g \\ -Q_1(\psi_2) + Q_2(\psi_2) \\ -Q_1(\nu_2) + Q_2(\nu_2) \\ -Q_1(\varphi_2) + Q_2(\varphi_2) \\ 0 \\ 0 \\ -m_2 g \\ -Q_2(\psi_3) + Q_3(\psi_3) \\ -Q_2(\nu_3) + Q_3(\nu_3) \\ -Q_2(\varphi_3) + Q_3(\varphi_3)] \end{bmatrix}, \tag{4.1}$$

where Q_1, Q_2 and Q_3 represent passive bending moments of shoulder, elbow and wrist, respectively.

Initial position of arm corresponding with an experiment is based on anthropometric data, namely a driver's position of holding the steering wheel. Initial condition of the arm is shown in fig 4.10.

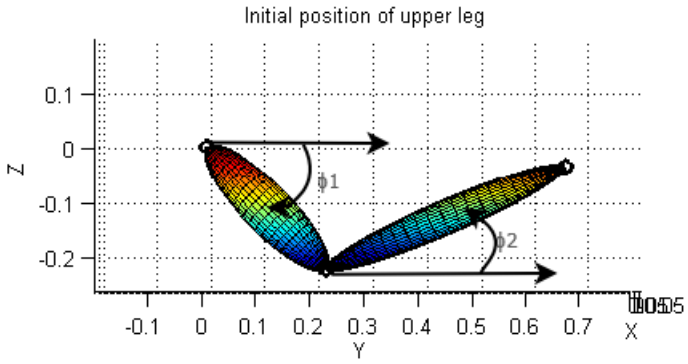

Figure 4.10: Initial position of arm

In which angles $\varphi_1 = -45°$ and $\varphi_2 = 23°$.

Results

First figure shows the motion of elbow of the right upper leg, see Fig 4.11. Where black solid curve represents the motion of the elbow in 3D double pendulum simulation, yellow dash-dot curve represents 2D simulation from [20] and red points represent motion during experiment [20].

Second graph, see Fig 4.12, shows the motion of a wrist. Curves and colors are the same with the previous figure.

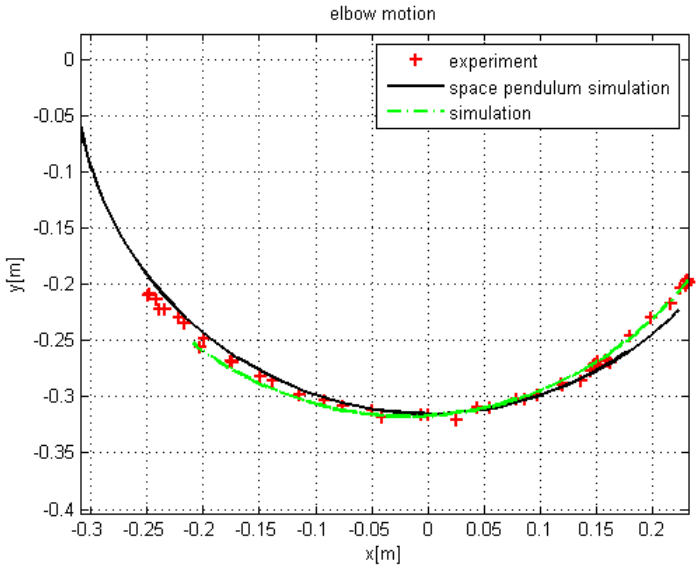

Figure 4.11: Comparison of trajectories of an elbow

Double pendulum system was compared with experiment and also with model based on 2D multibody approach. These systems represent free motion of right arm. In order to validate this particular model, comparison with experiment is highly desirable. Previous figures show that the motion of real arm is similar with simulated motion. Although the trajectory of the wrist slightly differs from the experiment and also from Valdmanova's simulation, it proves equivalence of systems. Valdmanová assumed the bodies with uneven mass distribution, but it was proved, that this assumption does not affect the results. To sum up results of this part, double pendulum system is validated to be appropriate system, representing a real human segment. Due to this detection, it can be applied in numerous applications.

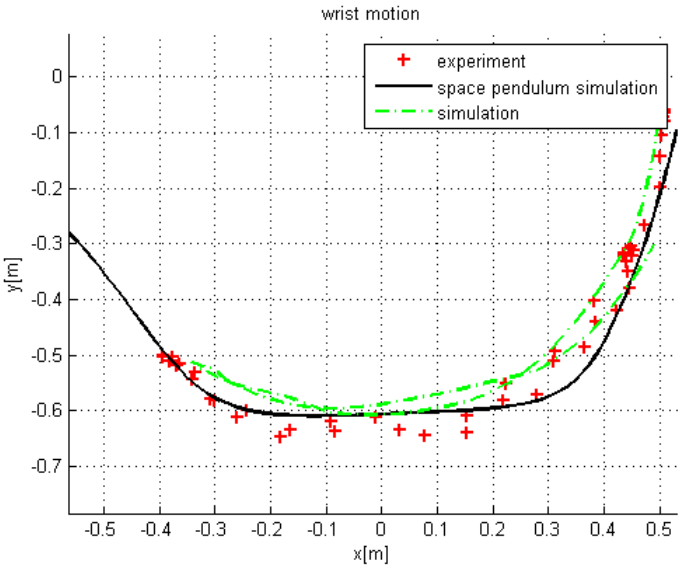

Figure 4.12: Comparison of trajectories of a wrist

4.3 Numerical optimization

In section 3.3 application of various solvers for numerical integration implemented in MATLAB software was described to solve equation of motion. Software optiSlang controls variation of input quantities, namely the contact parameters k and b, respectively, to reach the most corresponding results of simulation to an original experiment results. Principle of mathematics optimization was applied on all three normal contact force models.

4.3.1 Hertz's model

Since Hertz's model does not take energy dissipation effect into account, it can not reach a desired result. Whatever value of contact parameter k_h is set, the jump with the height equal to initial position is produced. By varying with k_h only an amount of penetration is changing. Figure 4.13 shows result of simulation with k_h equals to $1e5$ compared with original experimental result.

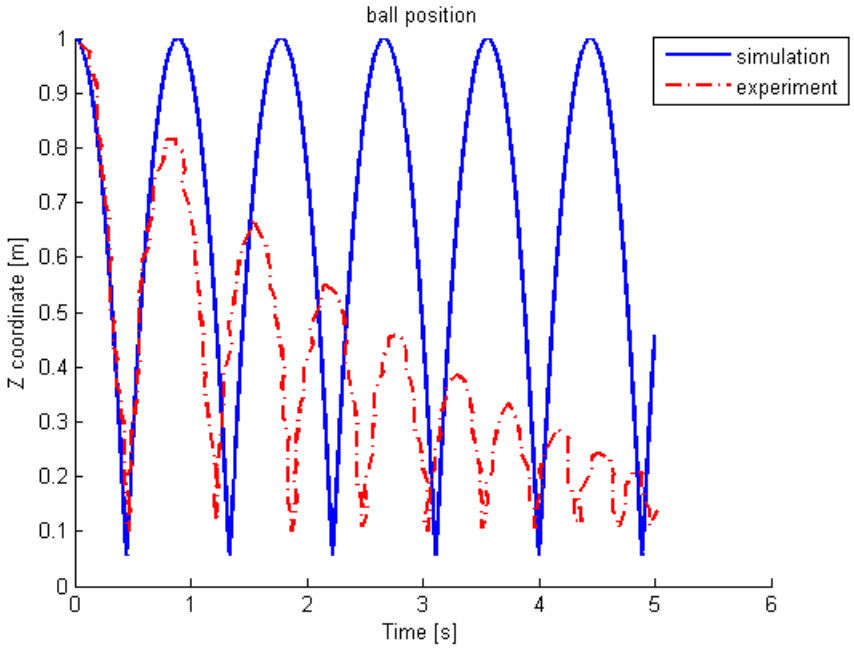

Figure 4.13: Result of bouncing ball example regarding Hertz's model for $k_h = 10000$

4.3.2 Spring-dashpot model

Spring-dashpot force model represents an example with linear spring in conjunction with linear damper. It refers to an elastic force and energy dissipation effects. Constants k_{sd} and b_{sd} represent imaginary spring stiffness and imaginary damping coefficient, respectively. Process of numerical optimization performed in optiSlang software varied with initial parameters k_{sd}, b_{sd} and calculated 722 simulations and the best one is displayed in Fig 4.14.

Value of the parameters of the *best design* are approximately equal to:

Parameter	Optimized value
k_{sd}	3.303e+7
b_{sd}	2.157e+4

Table 4.2: Parameters of best design for SD model

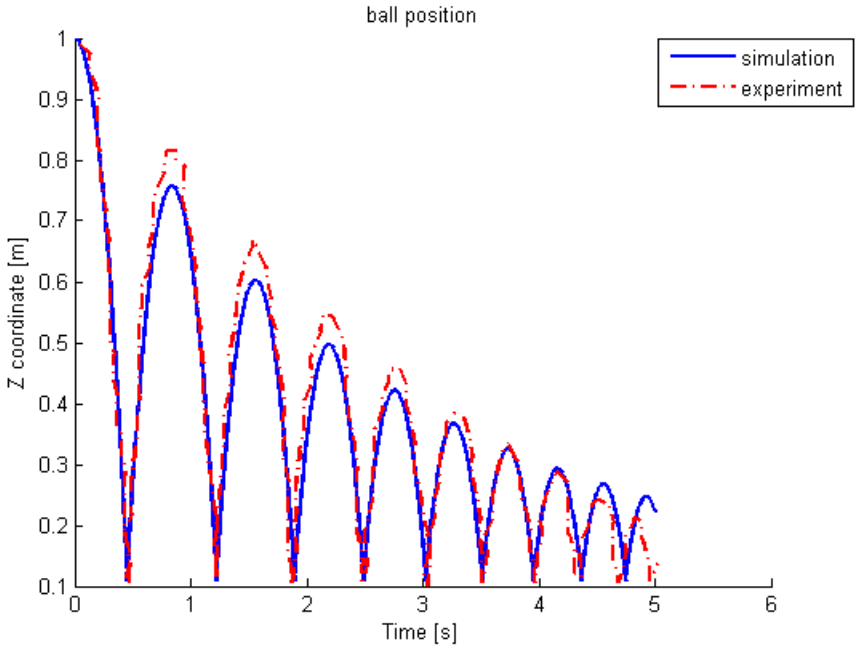

Figure 4.14: Result of bouncing ball example regarding Spring dashpot model

4.3.3 Non-linear model

Contact force model with non-linear damping element considers energy dissipation effect similar as with spring-dashpot model. This model dealt with the problems of discontinuities of contact force caused by damping term, that occur in the previous model. However, application of this contact force model may appear slightly unstable and ill-conditioned. Process of numerical optimization found an extrema after a few simulations. The obtained result does not correspond with an initial experiment as satisfactory as that of a spring-dashpot model simulation, see Fig 4.15. Several settings in optiSlang software were performed, varying in initial values and in parameters of optimization. Best results were achieved with those of equal to values shown in table 4.3. Results obtained in numerical optimization are displayed in Fig 4.15.

Parameter	Optimized value
k_{nl}	3.009e+7
b_{nl}	3.000e+4

Table 4.3: Parameters of best design for NL model

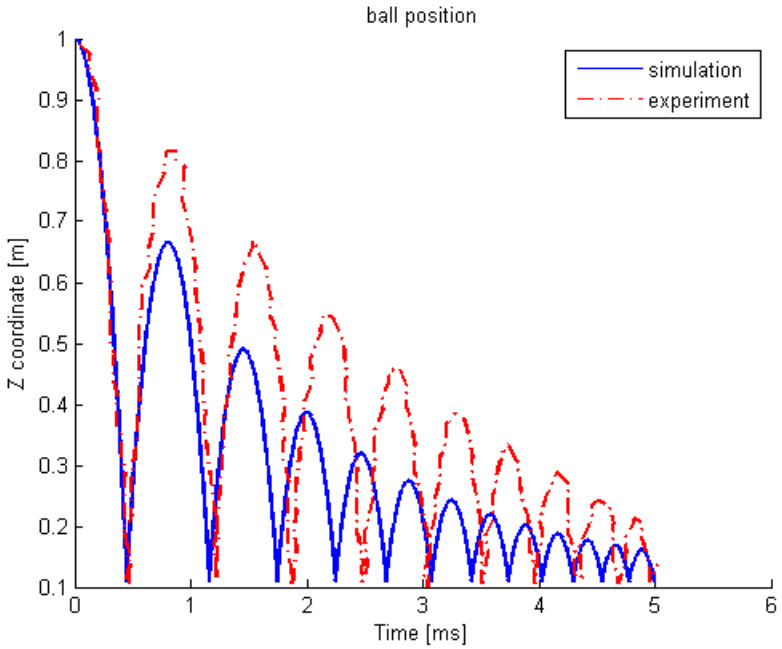

Figure 4.15: Result of bouncing ball example regarding non-linear damping model

4.3.4 Summary of optimization

Summarizing the knowledge and results obtained in process of numerical optimization of contact force parameters are reported in this part.

- Hertz's model performs an elementary model suitable for first approximation of an impact. Since it does not take energy dissipation phenomena into account, it is not applicable for all configurations. In case of a fully elastic impact, where coefficient of restitution approaching to one, this model can provide satisfactory results. Main advantages of Hertz model is resting upon its well-conditionality and simplicity.

- Spring-dashpot model includes damping coefficient to be a function of coefficient of restitution C_r. It refers to a more realistic situation, since it is not limited by elastic impact. Varying the parameters C_r between 0 and 1, phenomena between a fully plastic and a fully elastic impact are captured. Based on calculations, the spring-dashpot model provides results, most corresponding with an experiment. Thanks to this fact is applied in further calculations.

- Non-linear damping force model also works with dissipation of energy, but the conditioning of calculation can be discussed. One can observe that the curves of experiment and numerical simulation differ significantly, compared to spring-dashpot model. Calculation time of every single simulation in a process of optimization alters. This indicates an unstable problem.

4.4 Contact force

Very crucial question of impact is generated force. In generally, contact force represents a force with short duration time and with large amplitude. Maximum value of the contact force is highly important knowledge in evaluating of risk and injury of the bodies. As consequence of application in biomechanical examples, this might help in prediction of an injury of a human. However, there are no rupture criteria that can evaluate amount of deformation or injury as a function of the force. Nevertheless the knowledge of generated contact force can help in numerous fields.

Contact force diagram of bouncing ball example is presented in [9]. Here, this initial example force diagram is compared with the simulation. As consequence of previous results, the spring-dashpot model was applied. Both the force curves are displayed in Fig 4.16.

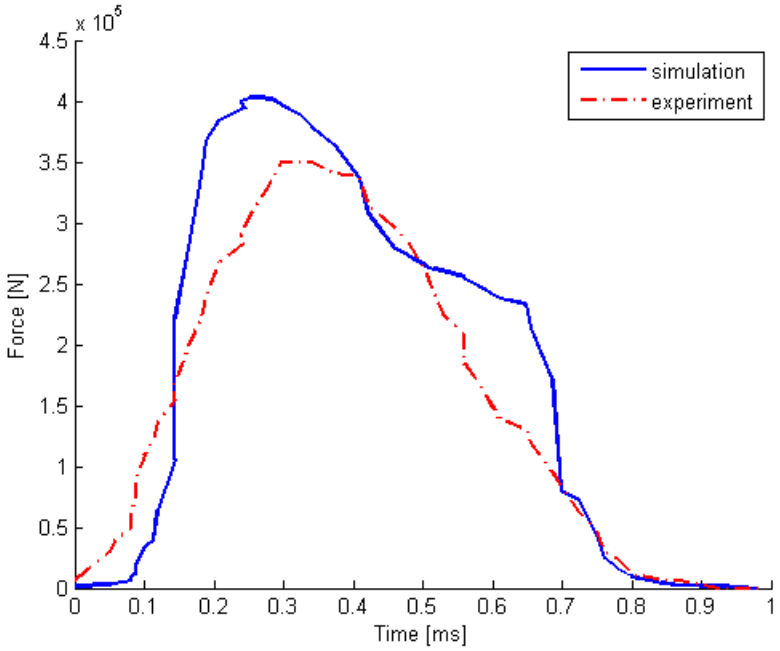

Figure 4.16: Contact force versus time

One can observe that both the curves have similar behaviour and also the maximum values are comparable. The maximum force and the deviation are shown in the table 4.4.

	Simulation	Experiment	Absolute deviation	Relative deviation
F_{Max}	4.032e5 [N]	3.496e5]N]	0.536e5 [N]	13.29 [%]

Table 4.4: Maximum values of contact force

4.5 Double pendulum contacting a plain

In previous section double pendulum system was described and validated to be a suitable approximation of a part of human body, namely the arm. Purpose of this part is to evaluate results of the system including a contact with general plain. Although this can be applied for example in approximation of an arm or a leg undergoing into an impact with a vehicle, here it is presented only to demonstrate a behaviour of the system. Further calculations may practise and validate double pendulum system in comparison with an experiment.

The presented system has parameters shown in table 4.5.

Parameter	Units	Body 1	Body 2
Moments of inertia $I_\psi = I_\nu = I_\varphi$	$[Kg.m^2]$	1	1
Length of semi-axes $a_1 = a_2$	$[m]$	1	1
Length of semi-axis a_3	$[m]$	2	2
Mass m	$[Kg]$	1	1

Table 4.5: Geometric parameters of the bodies

Results

Motion of double pendulum that gets into a contact with plain is displayed in t$\in [0, 1.25]$.

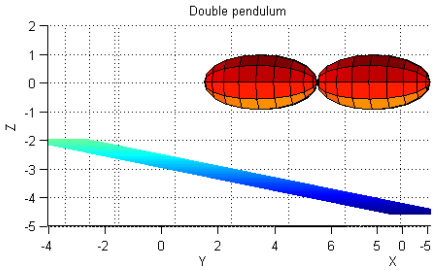

Figure 4.17: Position of double pendulum contacting a plain at t=0 sec

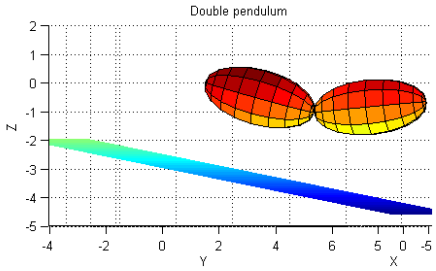

Figure 4.18: Position of double pendulum contacting a plain at t=0.25 sec

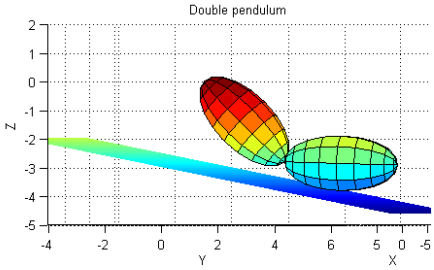

Figure 4.19: Position of double pendulum contacting a plain at t=0.5 sec

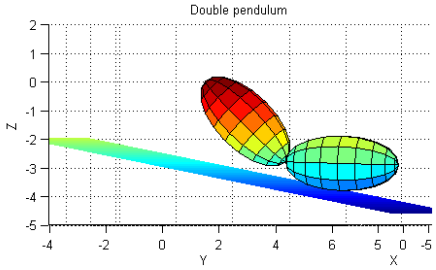

Figure 4.20: Position of double pendulum contacting a plain at t=0.75 sec

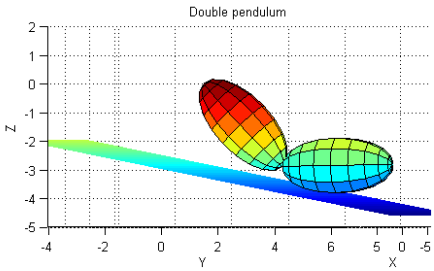

Figure 4.21: Position of double pendulum contacting a plain at t=1 sec

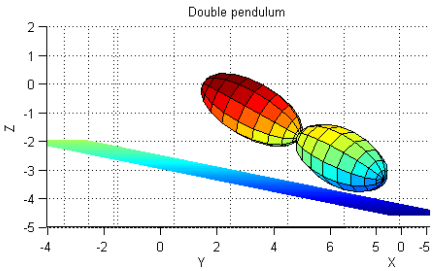

Figure 4.22: Position of double pendulum contacting a plain at t=1.25 sec

4.6 Legform impactor

Miyazaki in his work [11] presents development of a legform impactor in pedestrians safety testing. It considers steel shaft connected to metal plates to represent the femur and the tibia. It evaluates leg fracture risk based knee ligaments rupture risk based on knee bending angle and shear displacement. As a result, it can be used to help assess injury based on deformation by estimating the risk of tibia fracture from the bending moment of the tibia shaft and the risk of knee ligament rupture from the elongation of the wires.

System of two bodies constrained together can be gently applied in such a model of leg impactor. It can not fully approximate behaviour of a human leg and legform impactor, respectively. However, this can provide a first and elementary knowledge of after-impact motion. Geometry of the car can be improve to produces such a motion, that occurs a minimal risk of pedestrian's injury. Based on anthropometric data, kinematics joint between these two bodies is modelled to be a spherical joint with an internal stiffness. Thus the bodies load with a moment representing thickness of a knee, similarly with upper leg example. Passive bending moment curve of an elbow is used to approximate knee passive bending moment. Since elbow joint and knee are anatomically similar, this assumption should not bring any uncertainties. Zhou describes a leg impactor in his work [24]. Assuming a reference the overall geometric properties, it was determined that the optimal size of knee joint is a cylinder with a maximum diameter equal to 70mm. The human knee joint is like a spherical joint, in which all the three axes meet at the same point. However, the spherical joint might have great disadvantages compared to non-spherical ones. To realize 4-DOF joint, one can use 4 single joints, 2 double joints, 1 triple joint and 1 single joint or 1 quadruple joint. Based on previous research, Zhou realised knee joint structure consisting 1 double joint and 2 single joints, or two double joints, within appropriate internal stiffness, see Fig 4.23.

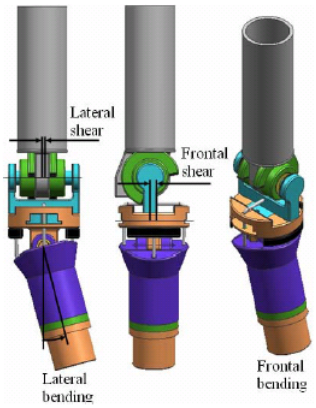

Figure 4.23: Experimental leg impactor [24]

Geometrical parameters of leg impactor based on [11] are defined in the table 4.23.

Where moments of inertia are calculated as moment of a cylinders adequate to [23].

Parameter	Units	Femur	Tibia
Length	$[mm]$	428	493
Diameter	$[mm]$	70	70
Mass m	$[Kg]$	8	4.8
Moments of inertia $I_\psi = I_\nu = I_\varphi$	$[Kg.m^2]$	0.033	0.0257

Table 4.6: Geometric parameters of leg impactor

Here, two ellipsoids jointed together approximate behaviour and after-impact motion of legform impactor. This work considers only contact with a plain, thus it is not comparable with experiment, in which impactor contacts a front part of the car. Experiment assumes the impactor exposure only with a gravity and moving in direction against car with initial velocity equal to 40 Km/h. These initial conditions are respecting in the simulation.

Results

Motion of two constrained ellipsoids that gets into a contact with plain is displayed in t$\in [0, 0.4]$ sec.

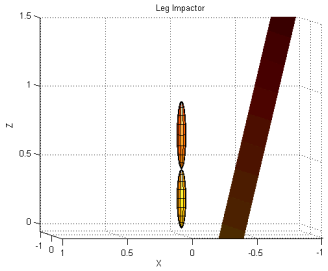

Figure 4.24: Position of leg impactor at t=0 sec

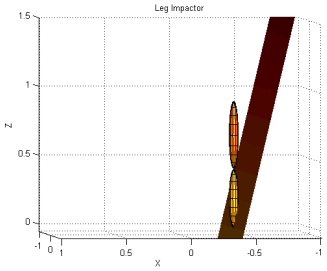

Figure 4.25: Position of leg impactor at t=0.05 sec

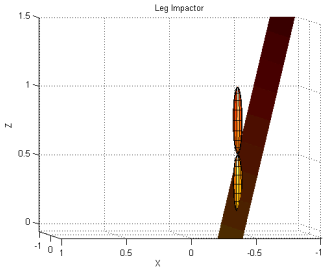

Figure 4.26: Position of leg impactor at t=0.1 sec

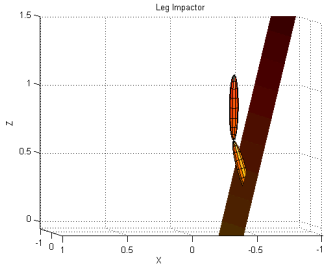

Figure 4.27: Position of leg impactor at t=0.15 sec

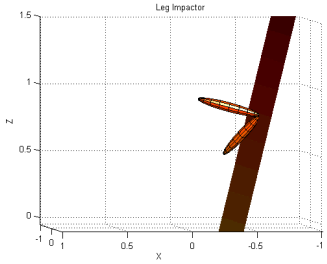

Figure 4.28: Position of leg impactor at t=0.2 sec

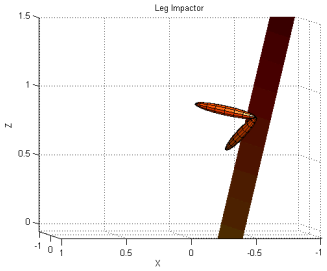

Figure 4.29: Position of leg impactor at t=0.25 sec

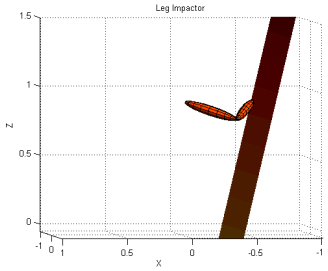

Figure 4.30: Position of leg impactor at t=0.3 sec

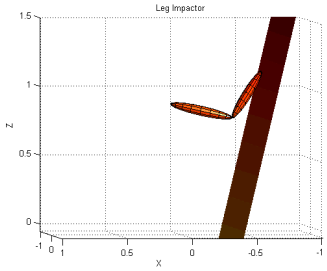

Figure 4.31: Position of leg impactor at t=0.35 sec

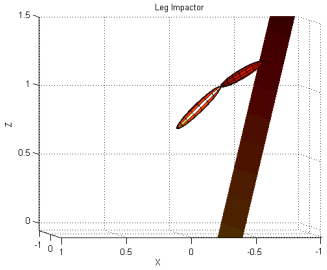

Figure 4.32: Position of leg impactor at t=0.4 sec

Chapter 5

Conclusion

Contact mechanics starts to be a very crucial phenomena in a various of engineering studies. Biomechanics contact problems, such as pedestrians accident, car crash, sports and impact injuries motivate engineers to develop and improve systems, that bring lower amount of risk and of injury. Anyone crossing the roads, driving a car or playing any sport is exposures to a biomechanics research as consequence of a possible impact.

Virtual human body modelling plays significant role of impact biomechanics research. Various of approaches in biomechanical modelling are currently developed. Model contains rigid bodies linked to open, or close, kinematics chain is based of multibody approach. Articulated rigid body system can provide a satisfactory model for the first approximation of a human behaviour. As consequence of simplicity of the model, rigid constrained approach can evaluate global long time behaviour of human in very short time. Detailed deformable models of human body can evaluate precise information about behaviour, deformations and injuries. These are limited with computation technologies. In many cases, multibody approach might identifies an adequate and sufficient information. Application of rigid body contact scenario deals with some crucial aspects. At the beginning, the selection of a suitable contact force model. Presently the continuous contact force models play significant role in various of applications. Idea of continuous contact model is that contact force is dependent on the amount of penetration between bodies and on the penetration velocity, respectively. Calculation of penetration can be very straight forward, for example distance between two spheres or highly complicated in case of irregular bodies. Various of analytical and numerical methods for distance calculation have been reported in literature overview. The very crucial aspect of continuous contact force model is evaluating of sufficient contact parameters. By varying the parameters, the most corresponding results of simulation to an original experiment can be achieved. Principle of numerical optimization can be applied to find such parameters. Multibody model can be loaded with contact force on each body independently. Mathematical constrains between bodies capture an effect of the bodies affecting one to each other.

The purpose of this thesis was to evaluate and test algorithm for system of a double pendulum getting into a contact with general plain. This work firstly presented literature

overview of contact detection algorithms and of contact force models. Later on, equation of motion of double pendulum according to multibody principle was derived. Problem in evaluation of contact force parameters was sorted out using numerical optimization principle applied on bouncing ball example. Three contact force models were investigated, namely the Hertz model, the spring-dashpot model and the nonlinear damping model. The optimized values of contact parameters together with graphical evaluations were presented and discussed. Assuming a reference of biomechanics research, the double pendulum system might approximate various segments of a human body. The applications of the arm and of the legfrom impactor based on multibody approach were verified here..

All the knowledge acquired during studies on this thesis can be easy applied in further researches. Contact detection algorithm can be modified and used in different bodies examples. Advantages and disadvantages of particular contact force models were pointed out and suitable applications of these models are discussed. It was proved that all the three models are a certain level of approximation of a real system and with particular contact parameters can be used in further applications.

Acknowledgment

I would like to express my gratitude to all those who gave me the possibility to complete this thesis. I want to thank the Department of Mechanics at the Faculty of Applied sciences. This work was supported by the inernal grant project SGS-2013-026.

I am deeply indebted to my supervisor Ing. Luděk Hynčík Ph.D. from University of West Bohemia who helped me in all the time of research for and writing of this thesis. I would like to express my thanks of gratitude to my consultant Ing. Michal Hajžman Ph.D. for valuable guidelines. They gave me the golden opportunity to work on this wonderful thesis on the topic of double pendulum contact problem, which also helped me in doing a lot of research and I discovered many new things. I am really thankful to them.

Secondly i would also like to thank my parents and friends who helped me a lot in finishing this project within the limited time.

Bibliography

[1] McPhee J. Boss, M. Volumetric contact dynamics model and experimental validation of normal forces for simple geometries. 2011.

[2] D. Eberly. Intersection of ellipsoids, 2010.

[3] G. Gilardi and I. Sharf. Literature survey of contact dynamics modelling. *Mechanism and Machine Theory*, 37:1213–1239, 2002.

[4] Hurmuzlu Y. Grahib, M. Correlation between impulse and compliance based methods in rigid body collisions. 2011.

[5] Tavakoli A. Hurmuzlu Y. Grahib, M. Kinematics and dynamics of a sliding/bouncing two mass system. 2011.

[6] M. Hajžman and P. Polach. Application of stabilization techniques in the dynamic analysis of multibody systems. *Applied and Computational Mechanics*, 1:479–488, 2007.

[7] K. H. Hunt and F. R. Crossley. Coefficient of restitution interpreted as damping in vibroimpact. *Journal of Applied Mechanics*, 42:440–445, 1975.

[8] L. Hynčík and H. Čechová. Car impact to pedestrian - fast 2d numerical analysis. *Applied and Computational Mechanics*, 2:151–162, 2011.

[9] M. F. Machado and P. Flores. A novel continuous contact force model for multibody dynamics. In *Proceedings ofthe ASME 2011 International Design Engineering Technical Conferences & Computers and Information in Engineering Conference IDETC/CIE 2011, year = 2011,.*

[10] MathWorks. MATLAB R2010a.

[11] H. Miyazaki, Y. Kitagawa, T. Yasuki, M. Kuwahara, and F. Matsuoka. Development of flexible pedestrian legform impactor FE model and comparative study with leg behavior of human FE model THUMS, journal = ESV Technical Paper 09-0112, year = 2009.

[12] Steffan H. Kasanický Moser, A. The pedestrians model in pc-crash-intorduction of a multi-body system and its validation. *SAE The engineering society for advancing mobility land sea air and space*, 1999.

[13] DesRoches R. Muthukumar, S. A hertz contact model with non-linear damping for pounding simulation. *Earthquake engineering and structural dynamics*, 35:811–828, 2006.

[14] F. Pfeiffer. Unilateral multibody dynamics. *Meccanica*, 34:437–451, 1999.

[15] F. Pfeiffer. On non-smooth dynamics. *Meccanica*, 43:533–554, 2008.

[16] F. Pfeiffer and C. Glocker. *Multibody dynamics with unilateral contacts*. Wilet-VCH GmbH & Co. KGaA, 2004.

[17] D. H. Robbins. Anthropometry of motor vehicle occupants. Technical report, 1983.

[18] Jttler B. Kim M.S. Wang W. Sohn, K.A. Computing distance between surfaces using line geometry. *IEEE Computer society*, 2002.

[19] Drexel University. The math forum @ drexel, 2010.

[20] L. Valdmanová. Model horní končcetiny ve 2d jako vázaný mechanický systém, 2009.

[21] W. Wang, Y. K. Choi, B. Chan, M. S. Kim, and J. Wang. Efficient collision detection for moving ellipsoids using separating planes. *Computing*, 72:235–246, 2004.

[22] Wikipedia. Heaviside step function, 2013.

[23] J. Zajíc. Momenty setrvavcnosti geometricky pravidelných homogenních těles. Technical report, 2010.

[24] Q. Zhou, M. Quade, and H. Du. Concept design of a 4-DOF pedestrian legform. *ESV Technical Paper 07-0196*, 2007.